Measurement report: Contrasting elevation-dependent ~~changes in~~ light absorption ~~of~~ by black and brown carbon: lessons from *in- situ* measurements from highly polluted Sichuan Basin to pristine Tibetan Plateau

Suping Zhao[1,2,3,4], Shaofeng Qi[1,6], Ye Yu[1,2,3], Shichang Kang[4], Longxiang Dong[1,2,3], Jinbei Chen[1,2,3], Daiying Yin[5,6]

[1] Key Laboratory of Land Surface Process and Climate Change in Cold and Arid Regions, Northwest Institute of Eco-Environment and Resources, Chinese Academy of Sciences, Lanzhou 730000, China
[2] Pingliang Land Surface Process & Severe Weather Research Station, Pingliang, 744015, China
[3] Gansu Land Surface Process & Severe Weather Observation and Research Station, Pingliang, 744015, China
[4] State Key Laboratory of Cryospheric Science, Northwest Institute of Eco-Environment and Resources, Chinese Academy of Sciences, Lanzhou 730000, China
[5] Key Laboratory of Desert and Desertification, Northwest Institute of Eco-Environment and Resources, Chinese Academy of Sciences, Lanzhou 730000, China
[6] University of Chinese Academy of Sciences, Beijing 100049, China

Correspondence to: Suping Zhao (zhaosp@lzb.ac.cn); Daiying Yin (yindaiying@lzb.ac.cn)

Abstract. The scientific knowledge on light absorption ~~of~~ by aerosols is extremely limited at the eastern slope of the Tibetan Plateau (ESTP). We conducted the first aerosol field experiment at six sites (Chengdu, Sanbacun, Wenchuan, Lixian, Maerkang, Hongyuan) along the ESTP ranging in elevation ~~extending elevation~~ from 500 m to 3500 m. The fraction of light absorption by brown carbon (BrC) to total carbon increases from 20%~~The light absorption of brown carbon (BrC) accounting for that of total carbon increases from 20%~~ to 50% with altitude, and the mass absorption efficiency (MAE) of BrC over the TP is 2–3 times higher than that inside the ~~SiChuan~~ Sichuan Basin (SCB), especially in winter. In contrast, the MAE of elemental carbon (EC) in winter decreases with altitude~~Contrary to BrC aerosols, winter EC (elemental carbon) mass absorption efficiency declines with altitude~~. The contrasting variation of EC and BrC MAE with altitude is mainly attributed to source difference between the TP and SCB. Emissions from the~~The~~ more urban sources (motor vehicles, industries, etc.) inside the SCB fail to be transported to the TP due to the stable air in winter inside~~to winter stable air inside~~ the basin, which ~~also~~ is also favorable for aerosol ageing to enhance absorption efficiency. The

radiative forcing of BrC relative to EC varies from 0.10 to 0.42 as altitude increases with the higher OC/EC ratio over the TP than SCB~~,~~. Thus, the reason of the enhanced relative BrC to EC radiative forcing from polluted SCB to pristine TP is that the BrC concentration decreases more slowly than the EC concentration with altitude~~and thus the enhanced radiative forcing of BrC relative to EC from polluted SCB to pristine TP is because the concentration of OC decreases more slowly with altitude than does EC~~. This study contributes to the understanding of the difference in light absorption by EC and BrC with altitude, from polluted lower-altitude basins to the pristine TP, and provides a data set for regional climate model validation.~~This study will deepen the understanding of EC or BrC light absorption difference between the highly polluted basins and clean TP and provide a basic data set for optimization of regional climate modeling.~~

1 Introduction

Some *in~~-~~ situ* observations, available satellite data, and model simulations indicate~~d~~ that a greate~~r~~ surface warming trend over time occurs at high~~er~~ altitudes in~~for~~ ~~the~~ mountainous regions worldwide~~all over the world~~ (Gao et al., 2018; Guo et al., 2019; Mountain Research Initiative EDW Working Group, 2015; Palazzi et al., 2017; Pepin et al., 2019; Rangwala and Miller, 2012; You et al., 2020). Rangwala and Miller (2012) reviewed elevation-dependent warming (EDW) and its possible causes over four high mountain regions~~, i.e.:~~; the Swiss Alps, ~~the~~ Colorado Rocky Mountains, ~~the~~ Tibetan Plateau (TP), and ~~the~~ Tropical Andes. The~~ir examinations found that the~~ available observations indicate that some mountain regions show ~~show~~ much greater warming rates at seasonal scales than others. The mechanisms that can produce enhanced warming rates at high~~er~~ altitudes may be related to the differential sensitivities of surface warming to changes in ~~the~~ climate drivers, ~~at different elevations,~~ such as snow-ice cover, clouds, atmospheric water vapour, aerosols, land use, and vegetation, at different elevations (Rangwala and Miller, 2012; You et al., 2020).

The ~~Tibetan Plateau (~~TP~~, hereafter)~~, known as the "'third pole"~~, '~~, is an ideal ~~place~~location to examine EDW and its mechanism (Guo et al., 2021). The warming rates (rising temperature per 10 years) over the TP we~~a~~re found to be the most notable in winter and autumn (Liu and Chen, 2000), especially for the central and eastern p~~P~~lateaus (Duan and Wu, 2006), which may be partly associated with human activities, such as more anthropogenic emissions in~~at~~ the sub-regions (Lu et al., 2010). The effect of

carbonaceous aerosols on regional and even global climate is more uncertain because~~due~~ of~~to~~ their shorter life than ~~the~~ long-lived aerosols~~ones~~, such as carbon dioxide and methane (Chung et al., 2012; Ramanathan and Carmichael, 2008). A~~The a~~bsorbing aerosols (black carbon and dust) from local emissions or long-range transport heat the atmosphere in two ways (Tian et al., 2018). They absorb radiation and decrease the surface albedo when deposited on snow and ice (Kang et al., 2019; Lau et al., 2010; Xu et al., 2009). Ramanathan and Carmichael (2008) suggested that black carbon (BC) in the Himalayas, arising from anthropogenic activities in~~at~~ the Indo-Gangetic Plain (IGP), could account for half of the local warming during the past several decades. In addition to the well-known BC, the recent work by Wu et al. (2018) suggested that the light absorption efficiency (LAE) of brown carbon (BrC, a certain type of organic aerosol~~s~~) in winter is 2~~–~~–3 times higher than that in summer for the central T~~ibetan~~ P~~lateau~~. However, ~~the~~ scientific knowledge o~~f~~n the optical properties of carbonaceous aerosols (elemental carbon (EC)~~EC~~, BrC) ~~is extremely limited~~ over ~~the~~ eastern TP is extremely limited, and *in* ~~-~~*situ* aerosol measurements at varying altitudes from the ~~the~~ heavily polluted Basin~~s~~ to the relatively clean TP a~~we~~re crucial ~~important~~ for better understanding their light absorption.

P~~The p~~revious *in* ~~-~~*situ* measurements have ~~mainly~~primarily focussed on the southern and northern slopes (Cong et al., 2015; Huang et al., 2007; Kang et al., 2020), whereas ~~ile~~ fewer observations have been~~were~~ conducted on~~at~~ the eastern slope of the TP (ESTP). The Si~~C~~chuan Basin (SCB)~~—~~, a highly polluted region in China caused by~~due to more~~ rapid economic development~~—~~, is located on the eastern side of the TP (Zhao et al., 2018). The BrC LAE was strong inside the Basin (Peng et al., 2020a), especially in~~for~~ ~~the~~ rural areas, because of ~~due to~~ increased~~more~~ biomass and coal burning impacts (Zhao et al., 2021). Our previous studies~~works~~ indicated that aerosols from the SCB are transported upslope along the ESTP and reach the eastern part of the TP by gradient *in* ~~-~~*situ* observations at the ESTP (Yin et al., 2020). The recent study by S. Y. Zhao et al. (2020) suggested the strong light-absorbing BrC from biomass and coal burning inside the Basin can be transported to the main part of the TP by the enhanced ~~“~~‘heat pump~~”~~’ in response to rapid warming over the TP. The aerosols over the TP from local emissions and long-range transport from the surrounding highly polluted areas affect~~ed~~ its weather, climate, and water cycle (C. F. Zhao et al., 2020). C~~The c~~louds and radiation are particularly sensitive to aerosols over pristine regions (Garrett and Zhao, 2006; Zhang et al., 2021). However, it is unclear~~fuzzy~~ whether~~that~~ the light absorption and radiative forcing of

carbonaceous aerosols change from ~~the~~ highly polluted SCB to ~~the~~ cleaner TP.

In this study~~work~~, we investigated the changes in the light absorption of carbonaceous aerosols (EC, BrC) and calculated the relative radiative forcing of BrC to EC aerosols from the SCB to TP in the four seasons. The sources and origins were also ~~were~~ determined ~~by~~ using ~~some~~ statistical methods and the hybrid single-particle Lagrangian integrated trajectory (HYSPLIT) ~~back trajectory~~ model. ~~Our goals are~~We aimed to understand the difference in EC or BrC light absorption ~~difference~~ between the highly polluted Basin~~s~~ and clean TP, ~~and~~ to reveal the ~~corresponding mechanisms~~causes of the difference, and to ~~provide~~ generate a basic data set for the optimi~~s~~zation of regional climate modelling.

2 Data and methods

2.1 Observation sites and aerosol sampling

Compared ~~with~~ to that of the coarser fraction of particulate matter (PM), the size of strong light-absorbing carbonaceous particles was~~are~~ ~~mainly~~primarily ~~located~~ in the submicron range. Therefore, samples ~~PM_1 (~~of particulate matter with an aerodynamic diameter smaller than 1 μm (PM_1) ~~samples~~ were collected at six sites (Chengdu, Sanbacun, Wenchuan, Lixian, Maerkang, and Hongyuan) from the western SCB to the east~~ern~~ part of the TP at elevations varying~~with varying elevation~~ from 500 m to 3500 m (Figure 1, Table 1). Each sampling site wa~~i~~s selected to represent the background level at the local scale as completely as possible, without local emission impacts. A total of~~The~~ 1024 PM_1 samples ~~in total~~ were collected from 21 December ~~21,~~ 2018 to 18 December ~~18,~~ 2019 on a day/night~~day / night~~ pattern using an~~by~~ aerosol sampler (LY-2034, Laoying Instrument Co., Ltd., China) at a~~the~~ flow rate of 100 L min^{-1}. The samples were stored frozen in pre-baked glass jars until further analysis (Kawamura et al., 2010). M~~The m~~eteorological variables (temperature, relative humidity, wind speed, and direction) were downloaded from~~by~~ the China Meteorological Data Service Center (http://data.cma.cn/). PM_1 samples were collected near ~~the~~ meteorological observation sites;~~,~~ ~~and~~ thus, the meteorological variables could~~can~~ represent the situation in~~at~~ the study region. ~~The~~ MODIS active fire data (https://earthdata.nasa.gov/active-fire-data) ~~also~~ were used in this study.

2.2 Chemical analysis

A quarter of each filter was used to analy~~s~~z~~z~~e water-soluble inorganic ions (Na^+, NH_4^+, K^+, Ca^{2+}, Mg^{2+},

F^-, Cl^-, SO_4^{2-}, and NO_3^-), and the ions were extracted and filtered usingby ultrapure water and a 0.45 μm pore syringe filter. The concentrations of the cations and anions were measured usingby ion chromatography (DX-600 & ICS-2500, Dionex, USA). CThe carbonaceous aerosols, that isi.e., organic carbon (OC) and ECelemental carbon (EC), were determined analysed usingby a seven-wavelength carbon analyszer (Model-2015, DRI, USA). The carbon analyszer measured the OC and EC concentrations using the thermal/optical reflectance (TOR) method (Chow et al., 2007). Briefly, the OC/ECOC / EC was determined by progressively heating the sub-filter. The OC fractions were determined by heating at 120 °C (OC1), 250 °C (OC2), 450 °C (OC3), and 550 °C (OC4) in a pure He atmosphere.; Thesubsequently, EC fractions were measured at 550 °C (EC1), 700 °C (EC2), and 800 °C (EC3) in an oxidiszing atmosphere of 2% O_2 and 98% He. -The carbon involved carbon is oxidiszed to CO_2 and then reduced to CH_4 for detection by a flame ioniszation detector. The pyrolyszed organic carbon (OPC) was monitored when the reflected laser signal returned to its initial value after the introductionintroducing of O_2 into the analysis atmosphere. The OC was defined as the sum of OC1, OC2, OC3, OC4, and OPC, whereas ile EC was defined as EC1 + EC2 + EC3 − OPC. The EC and BrC were derived from the light absorption coefficient (b_{abs}) depending on the transmittance attenuation. For the seven-wavelength carbon analyszer, the filter transmittance (FR_λ, fraction of light transmitted through the filter) uncertainties ranged from 5% to 18%, with the best precision observedshown at 450 nm and 808 nm (Chen et al., 2015). Thise uncertainty is attributed to the quality of the laser and the sensitivity of the photodiode detector for different wavelengths.

The coefficient of variation (CV), in conjunction with correlation coefficients (r), can be used to characteriszee the intra-location variability of chemical species (Zhao et al., 2021). The CV waiss calculated usingby the folbelowing equation:

$$CV_{jk} = \sqrt{\frac{1}{p}\sum_{1}^{p}\left(\frac{x_{ij} - x_{ik}}{x_{ij} + x_{ik}}\right)^2}, \quad (1)$$

where x_{ij} and x_{ik} are the average concentrations offor a chemical component i at sites j and k, respectively; and p is the number of samples. The CV values of zero and approaching one indicatemean no difference and absolute heterogeneity between the two sites for the specific chemical component, respectively. AThe CV lower than 0.2 is usually considered to represent a relatively similarity of spatial pattern (Wang et al., 2018).

2.3 Calculation of light absorption parameters

The BrC light absorption increases sharply as the wavelength decreases decreased wavelength, and thus, it can be separated from the EC (Peng et al., 2020a). The light absorption induced by carbonaceous aerosols (the sum of EC and BrC) on a quartz filter was estimated using by an algorithm of transmittance attenuation (*ATN*):

$$ATN_{\lambda} = \ln\left(\frac{FT_{\lambda,a}}{FT_{\lambda,b}}\right), \quad (2)$$

where, $FT_{\lambda,a}$ and $FT_{\lambda,b}$ in the right hand represent the filter transmittance after and before thermal analysis for the specific wavelength (λ), respectively. Referring to the work by Chen et al. (2015), the relationship between of ATN and with absorption optical depth (τ_a) can be given as follows:,

$$\tau_{a,\lambda} = a_{\lambda} \times ATN_{\lambda}^{2} + c_{\lambda} \times ATN_{\lambda} \quad (3).$$

This study used the two coefficients (a_{λ} and c_{λ}) reported by Chen et al. (2015). The light absorption absorption coefficients (b_{abs}) were can be calculated using the following with the equation:

$$b_{abs,\lambda} = \tau_{a,\lambda} \times \left(\frac{A}{V}\right), \quad (4)$$

where, *A* and *V* are the filter area and the sampling volume, respectively. The total b_{abs} can be separated into EC and BrC using by a simplified two-component model (Chen et al., 2015):

$$b_{abs,\lambda} = b_{abs,\lambda,EC} + b_{abs,\lambda,BrC} = K_1 \times \lambda^{-AAE_{EC}} + K_2 \times \lambda^{-AAE_{BrC}}, \quad (5)$$

where, K_1 and K_2 are fitting coefficients. AAE_{EC} and AAE_{BrC} represent the EC and BrC absorption Ångström exponents (AAE), respectively. They do not change as with wavelength. AAE_{EC} was assumed to be as 1 (Bond, 2001), and the other three parameters in Eq. (5) were obtained for AAE_{BrC} values between 2 and 8 with an the increment of 0.1, by least-square linear regression. T, and the AAE_{BrC} that led to the overall best fit in terms of R^2 was selected as the effective BrC AAE. The mass absorption efficiency (MAE) was obtained from by the ratio of light absorption coefficients ($b_{abs,\lambda,EC}$ or $b_{abs,\lambda,BrC}$) to the corresponding EC or OC mass concentrations (Olson et al., 2015). The estimated MAE_{BrC} was much lower than the true value by replacing BrC with OC, because due to BrC accounting for only a small fraction of OC. The main shortcoming of the separation of the total aerosol absorption into EC and BrC (Eq. 5) does not consider is lack of considering the mineral dust

impacts. According to athe recent study byof Zhang et al. (2021), mineral dust may be aimportant n-important atmospheric aerosol speciesspecies of the atmospheric aerosols over the Tibetan Plateau. However, the study region is located onat the eastern slope of the TP during our campaign, which is more easily affected by anthropogenic sources from the heavily polluted Sichuan CBasin than natural sources such as mineral dust (Yin et al., 2020) as compared to the northern areas close to the Taklimakan and Gobi Deserts. TheOne main aim of this study waiss to reveal the gradient distributions of aerosol optical properties from the pollution of the Sichuan SCBasin to the eastern TP;, and thus, the impact of thise shortcoming may be negligible when studying the spatial heterogeneity of aerosol optical properties at a relatively small spatial scale. In aAddionally, the AAE of EC waiss assumed to beas 1, and the ageingeing of EC was not consideredid not take when separating the total aerosol absorption into EC and BrC (Eq. 5) in our study.

The light absorbed light by the carbonaceous component can be estimated as follows (Huang et al., 2018):

$$\frac{I_0 - I}{I_0}(\lambda, EC) = 1 - e^{-\left(MAE_{\lambda 0,EC} \times \left[\frac{\lambda_0}{\lambda}\right]^{AAE_{EC}} \times C_{EC} \times PBLH\right)} \quad (6)$$

$$\frac{I_0 - I}{I_0}(\lambda, BrC) = 1 - e^{-\left(MAE_{\lambda 0,BrC} \times \left[\frac{\lambda_0}{\lambda}\right]^{AAE_{BrC}} \times C_{OC} \times PBLH\right)}, \quad (7)$$

where, 405 nm is thedetermined as reference wavelength λ_0, and C_{EC} and C_{OC} represent the EC and OC concentrations, respectively. The planetary boundary layer (PBL) height (PBLH) was obtained from the HYSPLIT model, and we assumed no vertical gradients were assumed within the PBL. Thise assumption might overestimate the radiative forcing of aerosols, while it that has a small effect on the radiative forcing of BrC relative to EC (*f*), which can be estimated usingby the folbelowing equation (Zhao et al., 2019):

$$f = \frac{\int I_0(\lambda)\left[\frac{I_0 - I}{I_0}(\lambda, BrC)\right] d\lambda}{\int I_0(\lambda)\left[\frac{I_0 - I}{I_0}(\lambda, EC)\right] d\lambda}, \quad (8)$$

where $I_0(\lambda)$ is the wavelength-dependent solar emission flux, which is the clear sky aAir mMass 1 gGlobal hHorizontal solar irradiance (Levinson et al., 2010). LThe light absorption by BrC at 405 nm and 445 nm is much stronger than that at the longer wavelengths inside the SCB (Zhao et al., 2021).

The 405 nm wavelength wasis the lower limit of detection ofby the DRI-2015 instrument of DRI 2015. Therefore, the fraction (*f*) wais obtained by numerical integration of the above formula inat the wavelength ranges of 405– 980 nm and 405– 445 nm for each sample, respectively. NThe nighttime samples were excluded when calculating the radiative forcing of the BrC relative to the EC.

The exponential function was selected to fit the relationships between BrC MAE and altitude (*AT*). The equation is given as follows:

$$MAE_{\lambda,BrC} = a_{\lambda} \cdot e^{b \times AT}, \quad (9)$$

where, a_{λ} and *b* are the fitted coefficients. The EC MAE can be parameterised with the altitude by replacing the subscript of *BrC* with *EC* in Eq. (9).

2.4 HYSPLIT backward trajectory model

The hyHYbrid sSingle pParticle Lagrangian iIntegrated tTrajectory (HYSPLIT) model developed by the National Oceanic and Atmospheric Administration's (NOAA) is a complete system for computing simple air parcel trajectories (Draxler et al., 2009). It HYSPLIT iscontinues to be one of the most extensively used atmospheric transport and dispersion models. A common application is a back-trajectory trajectory analysis to determine the origin of air masses and establish source-receptor relationships. In this study, the HYSPLIT model was used to determine the potential source regions of air pollutants during the four seasons at the six sites. The 96-h backward trajectories arriving at 500 m above ground level (AGL) and initialising at each hour of the day were calculated with the 0.25°×0.25° Global Data Assimilation System (GDAS) data from the National Centers for Environmental Prediction (NCEP). The gridded back-trajectory frequencies were calculated using thewith Openair package inof Rplot.

2.5 PMF receptor model

The EPA PMF receptor model (version: 5.0) is a mathematical approach for quantifying the contribution of sources to samples based on their composition or fingerprints of the sources. A specialisted data set can be viewed as a data matrix X of *i* ×by *j* dimensions, in which *i* number of samples and *j* chemical species were measured, with uncertainties *u*. The goal of the PMF model wais

to ~~solve~~ determine the chemical mass balance between the measured species concentrations and source profiles, as shown in ~~the below~~ Eq. (10), with the number of factors *p*, ~~the~~ species profile *f* of each source, and ~~the~~ amount of mass *g* contributed by each factor to each sample:

$$x_{ij} = \sum_{k=1}^{p} g_{ik} f_{kj} + e_{ij}, \quad (10)$$

where e_{ij} is the residual of each sample or species~~for each sample/species~~. In this study, the uncertainties of the chemical species concentrations were estimated ~~by~~ using~~the~~ Eq. (11):

$$Unc = \sqrt{(0.1 \times concentration)^2 + (0.5 \times MDL)^2}, \quad (11)$$

where MDL is the species-specific method detection limit. The water-soluble ions and carbonaceous aerosols in the four seasons at the six sites were used as input variables to run the PMF model. The MDL of the species can refer to Cui et al. (2019).

3 Results and discussion

3.1 Light absorption of EC and BrC

Table 2 summari~~z~~ses the seasonally mean OC and EC concentrations, light absorption coefficients, ~~and~~ efficiencies~~y~~ (b_{abs}, MAE) of EC and BrC at 405 nm, and the meteorological variables at the six sites during the campaign. The average winter EC concentration ranges from 2.2 μg m^{-3} at Maerkang to 7.9 μg m^{-3} at Sanbacun, which is ~~a bout~~ 2–6 times higher than that~~ose~~ in the other seasons in response to more primary emissions in winter with similar wind speeds (Table 2). The much higher OC/EC ratios at the Plateau sites than those ~~that~~ at the Basin sites suggest~~s~~ that more secondary OC is formed by chemical reactions over the TP, which has been corroborated by~~can be supported by the works of~~ Wu et al. (2018). H~~The h~~igh~~er~~ OC/EC ratios with increasing~~the~~ altitude can also result from strong~~er~~ EC emissions at low~~er~~ altitudes. Combined with those obtained from ~~the~~ previous studies, the winter OC concentration ~~i~~was found to vary from 15.0 to 20.1 μg m^{-3}, whereas ~~ile~~ EC ~~is~~ ranged between 4.3 and 4.7 μg m^{-3} at urban areas inside the SCB, which wa~~i~~s substantially ~~significantly~~ lower than that at the I~~ndo~~ G~~angetic~~ P~~lain~~ (Table S1). However, OC and EC concentrations in~~at~~ the eastern TP we~~a~~re much more abundant than those~~at~~ in~~at~~ the western and southern TP sites because~~due~~ of~~to~~ ~~the~~more dense~~r~~ population and widespread industrial activities~~y~~ (Table S1). ~~Briefly~~Thus, carbonaceous aerosol pollution is much more severe inside the Basin than ~~that~~ over the TP, indicating that ~~the~~ large amounts

of air pollutants areis trapped inside the deep Basin because of due to calm and stable air.

Figure 2 compares the spectral total and separated EC and BrC b_{abs} in spring and winter at the six sites along the ESTP. The measured (green hollow points) and calculated b_{abs} (yellow dashed lines) for total carbon ((TC,, –sum of EC and BrC) wereis comparable, and the difference waiswithin 5%. For Sanbacun, a rural site inside the Basin, the b_{abs} is much higher than the other sites, especially for the shorter wavelengths, because of due to more BrC emissions from coal and biomass burning for cooking and heating inat rural areas inside the SCB (Zhao et al., 2021). The light absorption of EC aerosols decreaseds with altitude, primarily because of the decreaslined EC concentration (see Table 2). Thise phenomenon may be partly due to caused by the stable air inside the deep Basin (Feng et al., 2020);, but however, itthat would also apply to BrC asin so far as EC and BrC share sources, and vertical mixing is primarily due to fair weather convection rather than deep convective storms (Zhang et al., 2017). However, the light absorption by BrC does not monotonically change withas altitude becausedue ofto the more complicated sources and origins of BrC. The 405 nm b_{abs} of BrC accounting for that of TC increaseds from 20% at Chengdu to ~ 50% at Hongyuan, whereas ile the proportion significantly reduceds with increasinged wavelength (Figure S1), suggesting that light absorption of BrC aerosols is much stronger at high altitudes than that at lowlands.

Compared towith b_{abs}, MAE can better reflect the LAElight absorption efficiency of aerosols. The average winter MAE_{EC} is 6.0±1.0 m^2 g^{-1} among all sites, which is within the range of 3.9–11.9 m^2 g^{-1} over the TP and the the surrounding basins (Tables 2 and S1). Except our result in the rural site, the mean winter MAE_{BrC} of 0.7–0.8 m^2 g^{-1} inside the SCB is approximately bout half of that at the Indo-Gangetic Plain (IGP) probably because of due to the differences in BrC emissions, PM size distribution and chemical composition between the SCB and IGP (Choudhary et al., 2018). Figures 3 and S2 show box plots of spectral MAE_{BrC} and MAE_{EC} in the four seasons from the Basin to Plateau sites, extending elevation from 0.5 to 3.5 km. In contrast toDifferent from EC, MAE_{BrC} at 405 nm over the TP waiswas 2–3 times higher than that inside the SCB with strong elevation-dependent light absorptionlight-absorbing, and the only clear dependence waiswas in winter. Wu et al. (2018) found that winter MAE_{BrC} waiswas 4.5 m^2 g^{-1} for a pristine environment over the TP (Nam Co, 4730 m asl), which is significantly higher than that at Hongyuan (3500 asl) infor our study. The average winter OC/EC ratio of 14.1 at Nam Co waiswas

significantly~~largely~~ higher than ~~that~~ at our sampling sites. Therefore, the clearly increased winter MAE_{BrC} with altitude may be related to BrC composition seasonally, whereas~~while~~ winter MAE_{EC} decreases with altitude, possibly because~~due~~ of~~to~~ the difference in source composition and ageing~~ing~~ aerosols inside the deep Basin (Liu et al., 2020). This~~e~~ mechanism is~~will be~~ discussed in the following sections.

Figure 4 shows MAE_{BrC} and MAE_{EC} variations as altitude in spring and winter during the campaign. The relationships between average MAE and altitude of the measurement sites were fitted by exponential function, and coefficients of determination (R^2) were given in the figure. R^2 reflects the strength of the relationships between two parameters. The contrasting MAE variation as altitude between BrC and EC in winter (R^2 of 0.89 for MAE_{BrC} and 0.86 for MAE_{EC}) is more significant than that ~~ose~~ in spring (R^2 of 0.45 for MAE_{BrC} and 0.06 for MAE_{EC}). The better relationships in winter may be because more urban and aged aerosols are trapped inside the deep Basin in response to strong winter temperature inversion (Feng et al., 2020). The relation of MAE_{BrC} or MAE_{EC} at 405 nm with altitude can be parameterised~~z~~ed with exponential function (Eq. 9). The spring and winter MAE_{BrC} can be parameteri~~z~~sed with altitude (*AT*) as follows:

$$MAE_{405,BrC,spr} = 1.33 \cdot e^{0.18 \cdot AT} \quad (12)$$

$$MAE_{405,BrC,win} = 0.82 \cdot e^{0.33 \cdot AT} \quad (13)~~.~~$$

Similarly, the winter MAE_{EC} can be parameterised~~z~~ed by altitude (*AT*) as follows:

$$MAE_{405,EC,win} = 11.35 \cdot e^{-0.18 \cdot AT} \quad (14)~~.~~$$

3.2 Sources impacting ~~on~~ the light absorption of EC and BrC

The OC/EC ratio can be used to approximate~~rough~~ly identify sources of carbonaceous aerosols, and the ratio of aerosols from fossil fuel combustion is generally lower than that from~~of~~ biomass burning (Bond et al., 2004). Figure S3 shows the relationship between OC and EC concentrations inside the SCB and ~~that~~ over the TP during the campaign, and the OC/EC ratio was obtained by fitting the relationships with univariate linear regression. The significantly simultaneous change between OC and EC (R^2 = 0.80 for SCB~~,~~ and R^2 = 0.75 for TP) indicated that the sources may be similar. The OC/EC ratios of 2.14 for western SCB and 2.06 for eastern TP are significantly lower than those~~at~~ at Nam Co

(13.8–14.1, Wu et al., 2018) representing a pristine environment over central TP (Cong et al., 2009), whereas ile the ratios are much higher than thoseat at Lhasa , the largest city of the ver TP (1.46, Li et al., 2016). The OC/EC ratios for in our study are is slightly lower than those at at for urban areas in eastern China and Helsinki in Finland (Han et al., 2014; Viidanoja et al., 2002), indicating that carbonaceous aerosols inat western SCB and eastern TP may be significantly affected by primary sources.

In addition toBesides primary sources, secondary formation largely contributes to OC aerosols;, and thus, secondary organic carbon (SOC) was calculated using thewith EC-tracer method (Turpin and Lim, 2001). To better understand the light absorption of primary organic carbon (POC) and secondary SOC, Figures S4 and 5 show sample-to-sample and average MAE_{BrC} variations as SOC and POC concentrations for each site in spring and winter during the campaign, respectively. The LAElight absorption efficiency of BrC significantly declineds as the increased OC composition increased with the better relationships for POC at each site (Figure S4). The average winter MAE_{BrC} decreased by approximatelyabout 70% as POC increasesd from 3.0 μg m^{-3} at Hongyuan to more higher than 20 μg m^{-3} at Chengdu (Figure 5). SOC accounting for OC significantly increaseds from the western SCB to the eastern TP, and it wasis higher than 50% at Maerkang and Hongyuan because of due to relatively fewer primary sources over the TP. The large winter MAE_{BrC} increment inas theas the SOC/POC ratio indicates that the more SOC and the fewer POC are is a favourable condition for BrC light absorption enhancement (Figure 5). Therefore, the strong elevation-dependent MAE_{BrC} in winter (Figure 4) may be induced by SOC/POC ratio variations from the western SCB to the eastern TP.

The EC LAElight absorption efficiency largely decreased as the reduces as EC concentrations increased at each site (Figure S5). However, the average winter MAE_{EC} inside the highly polluted SCB is was much higher than that over the clean TP, whereasile for similar EC concentrations among the Plateau sites, the MAE_{EC} at Wenchuan is was approximatelyabout two2 times higher than that at Hongyuan, with a strong dependence on elevation. Therefore, winter aerosol ageinging inside the deep Basin and large source differences may induce light absorption reduction from the western SCB to the eastern TP. The increase inof MAE_{EC} as the ratios of water-soluble ions (K^+, Cl^-, SO_4^{2-}, and NO_3^-) to EC concentrations aton different levels suggests that EC light absorption was affectedis certainly

~~impacted~~ by many anthropogenic sources at the six sites (Figure S6). A specific inorganic component can be considered ~~as an~~the indicator of a~~the~~ specific emission source~~s~~. K^+ and Cl^- ions are usually used to characterise~~for characterizing~~ biomass burning (BB) and coal combustion (CC), respectively (Tao et al., 2016). NO_3^- and SO_4^{2-} ~~can~~ reflect motor vehicle and industry source impacts, respectively. Therefore, to further identify the ~~find~~ key sources impacting MAE_{EC}, we ~~checked~~ verified the spring and winter mean MAE_{EC} variations as the concentrations of K^+, Cl^-, NO_3^-, and SO_4^{2-} ions at the six sites (Figure 6). Compared ~~with~~ to the spring value, the winter MAE_{EC} was ~~is the~~ lower owing~~due~~ to high EC concentrations and was ~~is~~ more sensitive to ~~the~~ the chemical species from anthropogenic emissions. Furthermore, the NO_3^- difference among the sites (Figure 6a) wa~~i~~s much larger than that of K^+, Cl^-, and SO_4^{2-} because of ~~due to~~ the combustion of fossil fuels~~many fossil fuel combustion~~ at the Chengyu City Clusters inside the Basin. The spatial heterogeneity in the $(NO_3^- + SO_4^{2-})$-/-$(K^+ + Cl^- + NO_3^- + SO_4^{2-})$ ratio in winter wa~~i~~s more significant than that in spring, and winter MAE_{EC} evident~~obvious~~ly increase~~d~~s as the ratio from the TP to ~~the~~ Basin sites. Therefore, ~~the~~ emissions from fossil fuel combustion may be a key ~~source~~ influence on ~~ing~~ winter MAE_{EC}.

The above paragraphs separately analyse~~analyzed~~ the LAE~~light absorption efficiency~~ of BrC and EC and their variations as chemical species, ~~while~~ and the change in radiative forcing of BrC relative to EC (*f*) from Chengdu to Hongyuan is shown~~ed~~ in Figure 7a to reveal the mechanism. P~~The p~~arameter (*f*) reflects the light absorption strength of BrC at ~~the~~ shorter wavelengths ~~as~~ compared to that of EC aerosols at all ~~the whole~~ wavelengths. The much higher *f* values indicate~~d~~ that the radiative forcing of BrC aerosols is much stronger for ~~the~~ similar EC radiate forcing~~;, and~~ thus, this parameter can be used to better understand the radiative forcing of secondary aerosols relative to primary aerosols at a specific location. The altitude (*AT*) increased by 3 km, and~~while~~ the median *f* increase~~d~~s from approximately~~about~~ 0.10 inside the Basin to 0.42 over ~~the~~ eastern TP. The relationship between *f* and altitude can be parameteri~~z~~sed as follows~~the below equation~~:

$$f = 0.077 \cdot e^{0.480 \cdot AT} \quad (15)$$~~.~~

~~Some~~ A few studies have found that the direct radiative forcing of BrC-/-(BrC+EC) increases with altitude ~~simply~~ because~~due to the fact that~~ the concentration of BrC decreases more slowly with altitude ~~than~~ than that of ~~does~~ EC (Liu et al., 2014, 2015; Zeng et al., 2020; Zhang et al., 2017).

Therefore, we also checked the median OC/EC ratio variations from the Basin to ~~the~~ Plateau sites during the campaign (Figure 7b). The OC/EC ratio change~~d~~s within the range of 2–4, and the 75th percentile~~s~~ of the ratio increase~~d~~s more significantly than the median values from the Basin to Plateau sites. Therefore, the increased *f* from ~~the~~ western SCB to ~~the~~ eastern TP may be closely related to more secondary formation and fewer primary emissions over the TP than over the SCB (also see Figure 5c).

As previously mentioned, the MAE of carbonaceous aerosols largely depends on emission sources. The PMF receptor model is widely used to apportion the sources influencing air pollutants at a specific site based on the fingerprints of the sources~~;~~, for example, K^+ and Cl^- are usually used as tracers for BB~~biomass burning (BB)~~ and CC~~coal combustion (CC)~~, respectively (Tao et al., 2016). The PMF analysis was conducted in this study for each season. M~~The m~~otor vehicles, biomass and coal burning, dust, sea salt, and secondary formations wea~~r~~e found to be the main sources at the six sites. Figure 8 shows mass concentrations of species for each source at each site apportioned using the~~by~~ PMF model in winter during the campaign. The PMF results for the other seasons are shown~~illustrated~~ in Figures S7–S9. The winter NO_3^- concentrations for secondary nitrate decreased from 3.44 μg m^{-3} in~~at~~ Sanbacun to 0.07 μg m^{-3} in~~at~~ Maerkang, which is more heterogeneous than that in summer and fall. As a main source inside the SCB, the winter secondary nitrate is in response to the intensive mixing between ~~the~~ motor vehicle emissions and other primary pollutants trapped inside the Basin by strong capping inversion (Feng et al., 2020). Additionally, high humidity inside the SCB facilities ~~the~~ secondary nitrate formation, and the average nitrogen oxidation ratio in Sichuan (average RH = 80%) is 3.1 times of that in winter in Beijing (average RH = 27%) (Wang et al., 2021). EC aerosols from ~~the~~ intensive human activities inside the SCB are easily aged by coating the secondary~~-~~-formed nitrate in winter, which further ~~causes the~~ enhance~~ment of thes~~ Basin EC light absorption. The latest ~~studies~~ study by~~of~~ Zhang et al. (2022) found that ~~the~~ light absorption and radiative forcing of BC~~black carbon~~ coated with~~by~~ inorganic salts are much stronger than of that inside organic materials. The chemical species (K^+, Cl^-) from BB~~biomass burning~~ and CC~~coal combustion~~ decline~~d~~ from the Basin to Plateau sites; however,~~but~~ the declining ranges in the warm seasons (summer and fall) were ~~are~~ more significant than those in the cold seasons (spring and winter) because of the use~~due to usage~~ of more fuel for heating over the TP. Therefore, the primary BrC from BB~~biomass burning~~ and CC~~coal combustion~~ for winter heating over the TP may partly contribute to ~~the~~ strong TP BrC light absorption.

3.3 Impacts of regional and long-range transport on the light absorption of aerosols

FThe fresh aerosol particles are gradually aged by mixing with other pollutants during the long-range transport, and thereby enhancinge their light absorption and radiative forcing. The similarities of the major chemical species between the two sites should represent regional air pollution, whereas ile the differences should reflect local source impacts. The comparisons between Basin (Chengdu, Sanbacun) and Plateau sites (Wenchuan, Lixian, Maerkang, Hongyuan) related to about the average mass concentrations of water-soluble ions and carbonaceous species in the four seasons are showed shown in Figures 9 and S10–S12. The numerical ranges between the two axes of each subplot weare set to be equal to more clearly observe the spatial heterogeneity of the chemical species inat the region. The combination of the CV andwith correlation coefficients can be used to better understand intra-location variability (Wilson et al., 2005). The CV wais between 0 and 1 (see Eq. 1), whereand athe smaller value representeds athe more uniform particle concentrations. MThe moderate differences and, relatively high CV values (0.22–0.75) were, are observed for the chemical species from anthropogenic sources (NH_4^+, K^+, SO_4^{2-}, NO_3^-, F^-, Cl^-, OC, and EC) in the four seasons. The differences indicated that there weare limited similarities between the Basin and Plateau sites, and the discrepancies were in major anthropogenic sources. The spatial heterogeneity offor K^+ and NO_3^- is more obvious evident than that of the other species in the four seasons, which is mainlyprimarily related to more BBbiomass burning and vehicle emissions inside the SCB (Zhao et al., 2021). The weak inter-regional transport between the western SCB and eastern TP suggested that the light absorption of carbonaceous aerosols over the TP is rarely influenced by pollutants from the SCB. Furthermore, the CV values for K^+, NO_3^-, and EC in winter weare the lowest among the seasons becausedue ofto increased BBbiomass burning and CCcoal combustion for winter heating over the Tibetan Plateau. Unlike CV, a high correlation coefficient for athe specific chemical component does not necessarily indicate uniformity, which may suggest source similarity between sites. The correlation largely dependeds on the season (Figures 9 and S10–S12). The strong correlations for NH_4^+, K^+, SO_4^{2-}, NO_3^-, OC, and EC in the spring and winter implied yinfer that Basin and Plateau sites shared similar sources for the species, whereaswhile weak correlations for NO_3^-, OC, and EC in summer and fall indicated impacts of dissimilar sources impacts between the Sichuan SCBasin and Tibetan Plateau.

Compared towith the species from anthropogenic sources, the lowest CV values for Na^+, Mg^{2+}, and Ca^{2+} among the species indicated that they weare more comparable between the Basin and Plateau sites. Furthermore, changes in Na^+ values weare more synchronous than those of Mg^{2+} and Ca^{2+} in the summer and fall. Na^+ concentrations wereis found to be high in salt-rich dust from saline soils (Quick and Chadwick, 2011). Dust events frequently occurred in spring and winter over the Tibetan PlateauP and northwest China, where saline and alkaline land and dried salt--lakes are located (Jiang et al., 2021; Zhang et al., 2009; Zhang et al., 2021),). and Tthus, the weak correlations for Na^+, Mg^{2+}, and Ca^{2+} values in spring and winter may suggest local and regional dust plume impacts. Therefore, the lack of considering mineral dust impacts in separation of BrC light absorption from total aerosol absorption (Eq. 5) might cause some errors. The errors should be much smaller as than those ofcompared to the studies onat the north or northeast TP close to the Taklimakan and Gobi Deserts.

MODIS active fire data suggests that BBbiomass burning is mainlyprimarily loconducated in South Asia around our study regions, which wais more abundant frequent in cold than warm seasons during our campaign (Figure S13). The PM mass concentrations in conjunction with wind data can be used to identify the local PM origins., and Figure 10 shows that K^+ pollution increasedrose in the four seasons at the six sites. The back--trajectory calculation can providegive PM origins from long-range transport., and Figures 11 and S14--S16 illustrate the gridded back--trajectory frequencies in the four seasons. K^+ stratification in warm seasons is was more obvious evident than that in cold seasons, which implyingsinfers that there were are substantial more BBbiomass burning plumes over the Tibetan PlateauP in spring and winter. The change in wind direction is not obvious from the Sichuan SCBasin to the TPibetan Plateau during warm seasons is not evident. However, the predominant wind direction is northwest–southeast in cold seasons for the Basin sites, whereaswhile itthat mainlyprimarily focusses on the southwest for the Plateau sites (Figure 10). The highest frequency of the back trajectory was also is in the southwest of the sampling sites in winter (Figure 11). Therefore, the BBbiomass burning emissions originatinged from South Asia are transported to the eastern Tibetan PlateauP by highly frequent southwesterly winds, and thus inducinge high K^+ concentrations in spring and winter. The BrC aerosols from the intensive BBbiomass burning in South Asia are gradually aged by internal or external mixing with the other anthropogenic emissions during the long-range transport. The light absorption of the aged BrC aerosols over the TP is enhanced by coating withe inorganic components (Zhang et al.,

2022), which may partly contribute to ~~the~~ stronger BrC light absorption at the Plateau sites than that at the Basin sites. Unlike ~~the~~ eastern TP, the carbonaceous aerosols in ~~the~~ western SCB are regionally transported from ~~the~~ central and eastern SCB, as~~which~~ can be seen from the increase in pollution ~~rose~~ and back trajectories. The aerosols accumulate and stagnate at the front areas of the mountains because of ~~due to~~ the terrain block~~;~~, ~~and~~ thus, ~~the~~ light absorption ~~of~~by EC aerosols emitted from motor vehicles is enhanced by the intensive mixing among the air pollutants.

4 Summary and conclusions

Tibetan Plateau ~~(TP)~~ is surrounded by the three highly polluted regions, i.e., ~~Indo-Gangetic Plain (~~IGP~~)~~, Taklimakan and Gobi Deserts (TGDs) and ~~SiChuan Basin (~~SCB~~)~~. However, ~~the~~ previous studies have ~~mainly~~ primarily focussed on the south (IGP) and north slopes (TGDs)~~.~~, ~~and thus t~~The first *in -situ* aerosol measurements were conducted ~~at~~ on the ~~eastern slope of Tibetan Plateau (~~ESTP~~)~~ to study the elevation-dependent light absorption ~~of~~ by carbonaceous aerosols from the highly polluted SCB to the pristine TP. The source and origin impacts on light absorption ~~of~~ by aerosols ~~also~~ were also discussed by combining with PMF and HYSPLIT results.

The EC and BrC light absorption~~s~~ were~~was~~ separated using~~by~~ a~~the~~ simple two-component model. The BrC light absorption coefficient at 405 nm, accounting for that of ~~total carbon (~~TC~~,~~ (sum of EC and BrC), was ~~is~~ found to increase from ~ 20% inside the SCB to ~ 50% over the TP. The BrC ~~mass absorption efficiency (~~MAE~~)~~ over ~~the~~ eastern TP wa~~i~~s 2–3 times higher than that inside the SCB, with strong elevation-dependent absorption. The most significant elevation-dependent winter MAE_{BrC} was ~~is~~ closely related to the high ratio of SOC to POC~~secondary to primary organic carbon (OC)~~, that is~~i.e.~~, more OC from secondary formation than those from primary emissions at high altitudes. In contrast to~~Different from~~ BrC, winter MAE_{EC} decline~~s~~d from the highly polluted SCB to the clean TP ~~, which is because of due to~~ source differences between the two regions. Substantial ~~More~~ urban ~~sources~~ emissions (vehicles, industries, etc.) ~~are~~ were trapped inside the deep SCB owing~~due~~ to poor dispersion and frequent temperature inversion during cold seasons. H~~The h~~igh primary emissions and weak dispersion conditions were ~~are~~ favourable for mixing and aerosol ageing~~ing~~ to enhance ~~the~~ light absorption inside the Basin. The median radiative forcing of BrC relative to EC increase~~s~~d from approximately~~about~~ 0.10 inside the Basin to 0.42 over ~~the~~ eastern TP, which was ~~is~~ associated with the

OC/EC ratio. Therefore, the enhanced radiative forcing of BrC relative to EC occurredsis because OC the concentration of OC decreased more slowly with altitude than the than does EC concentration.

The first aerosol field experiment was conducted inat athe specific study region; however, but only six sampling sites were used from the deep SCB to the eastern TP were used in this study. MThe more measurement sites shouldwill be established to better understand the chemical composition and light properties of aerosols inat athe unique region. The light absorption coefficients and efficiencies of BrC could not failed to be separated from thoseat of TC in summer and fall at Maerkang and Hongyuan because of due to instrument failure, which limited the revelation o revealof the elevation-dependent light absorption. Furthermore, replacing BrC, OC mass concentration was used to estimate MAE_{BrC}, which may cause significant large uncertainty; , and thus these are expected to be corrected in the future studiesy.

Data availability. Raw data sets (Zhao et al., 2022, DOI: 10.5281/zenodo.6474199) used in this manuscript were available at https://zenodo.org/record/6474199#.YmCn_YtByUk.

Author contributions. Suping Zhao and Ye Yu designed the study. Suping Zhao analyzed the data with help from Ye Yu, Jinbei Chen and Shichang Kang. Daiying Yin and Longxiang Dong collected and analyzed data during the campaign. Shaofeng Qi conducted the field experiment.

Competing interests. The authors declare that they have no conflict of interest.

Financial support. This work was supported by the National Natural Science Foundation of China (42075185; 41605103), Youth Innovation Promotion Association, CAS (Y2021111), and Gansu Science and Technology Program key projects (20JR10RA037 and 18JR2RA005).

References

Bond, T. C.: Spectral dependence of visible light absorption by carbonaceous particles emitted from coal combustion, Geophysical Research Letters, 28(21), 4075–4078, 2001.

Bond, T. C., Streets, D. G., Yarber, K. F., Nelson, S. M., Woo, J. H., and Klimont, Z.: A technology-

based global inventory of black and organic carbon emissions from combustion, Journal of Geophysical Research: Atmospheres, 109(D14), D14203, 2004.

Chen, Y., Xie, S. D., Luo, B., and Zhai, C. Z.: Characteristics and origins of carbonaceous aerosol in the Sichuan Basin, China, Atmospheric Environment, 94, 215–223, 2014.

Chen, L. W. A., Chow, J. C., Wang, X. L., Robles, J. A., Sumlin, B. J., Lowenthal, D. H., Zimmermann, R., and Watson, J. G.: Multi-wavelength optical measurement to enhance thermal/optical analysis for carbonaceous aerosol, Atmospheric Measurement Techniques, 8(1), 451–461, 2015.

Chen, P. F., Kang, S. C., Tripathee, L., Ram, K., Rupakheti, M., Panday, A. K., Zhang, Q. G., Guo, J. M., Wang, X. X., Pu, T., and Li, C. L.: Light absorption properties of elemental carbon (EC) and water-soluble brown carbon (WS–BrC) in the Kathmandu Valley, Nepal: A 5-year study, Environmental Pollution, 261, 114239, 2020.

Choudhary, V., Rajput, P., Singh, D. K., Singh, A. K., and Gupta, T.: Light absorption characteristics of brown carbon during foggy and non-foggy episodes over the Indo-Gangetic Plain, Atmospheric Pollution Research, 9(3), 494–501, 2018.

Chow, J. C., Watson, J. G., Chen, L.-W. A., Chang, M. C. O., Robinson, N. F., Trimble, D., and Kohl, S.: The IMPROVE_A Temperature Protocol for Thermal/Optical Carbon Analysis: Maintaining Consistency with a Long-Term Database, Journal of the Air & Waste Management Association, 57(9), 1014–1023, 2007.

Chung, C. E., Ramanathan, V., and Decremer, D.: Observationally constrained estimates of carbonaceous aerosol radiative forcing, Proceedings of the National Academy of the Sciences of the United States of America, 109(29), 11624–11629, 2012.

Cong, Z. Y. , Kang, S. C., Smirnov, A., and Holben, B.: Aerosol optical properties at Nam Co, a remote site in central Tibetan Plateau, Atmospheric Research, 92(1), 42−48, 2009.

Cong, Z. Y., Kang, S. C., Kawamura, K., Liu, B., Wan, X., Wang, Z., Gao, S., and Fu, P.: Carbonaceous aerosols on the south edge of the Tibetan Plateau: concentrations, seasonality and sources, Atmospheric Chemistry and Physics, 15(3), 1573–1584, 2015.

Cui, X. Q., Ren, J. W., Wang, Z. B., Yu, G. M., and Yue, G. Y.: Soluble ions in atmospheric $PM_{2.5}$ over glacier terminus determined by ion chromatography and source analysis, Journal of Glaciology and Geocryology, 41(3), 574–578, 2019 (in Chinese).

Duan, A. M., and Wu, G. X.: Change of cloud amount and the climate warming on the Tibetan Plateau,

Geophysical Research Letters, 33(22), L22704, 2006.

Draxler, R., Stunder, B. Rolph, G., Stein, A., and Taylor, A.: Hybrid Single–Particle Lagrangian Integrated Trajectories (HYsplit): Version 4.9–User's Guide and Model Description, 2009.

Feng, X. Y, Wei, S. M, and Wang, S. G.: Temperature inversions in the atmospheric boundary layer and lower troposphere over the Sichuan Basin, China: Climatology and impacts on air pollution, Science of the Total Environment, 726, 138579, 2020.

Gao, Y. H., Chen, F., Lettenmaier, D. P., Xu, J. W., Xiao, L. H., and Li, X.: Does elevation-dependent warming hold true above 5000 m elevation? Lessons from the Tibetan Plateau, npj Climate and Atmospheric Science, 1, 19, 2018.

Garrett, T. J., and Zhao, C. F.: Increased Arctic cloud longwave emissivity associated with pollution from mid-latitudes, *Nature*, 440(7085), 787–789, 2006.

Guo, D. L., Sun, J. Q., Yang, K., Pepin, N., and Xu, Y. M.: Revisiting recent elevation-dependent warming on the Tibetan Plateau using satellite-based data sets, Journal of Geophysical Research: Atmospheres, 124(15), 8511–8521, 2019.

Guo, D. L., Pepin, N., Yang, K., Sun, J. Q., and Li, D.: Local changes in snow depth dominate the evolving pattern of elevation-dependent warming on the Tibetan Plateau, Science Bulletin, 66(11), 1146–1150, 2021.

Han, T. T., Liu, X. G., Zhang, Y. H., Gu, J. W., Tian, H. Z., Zeng, L. M., Chang, S.-Y., Cheng, Y. F., Lu, K. D., and Hu, M.: Chemical characteristics of PM_{10} during the summer in the mega-city Guangzhou, China, Atmospheric Research, 137, 25–34, 2014.

Huang, J. P., Minnis, P., Yi, Y. H., Tang, Q., Wang, X., Hu, Y. X., Liu, Z. Y., Ayers, K., Trepte, C., and Winker, D.: Summer dust aerosols detected from CALIPSO over the Tibetan Plateau, Geophysical Research Letters, 34(18), L18805, 2007.

Huang, R. J., Yang, L., Cao, J. J., Chen, Y., Chen, Q., Li, Y. J., Duan, J., Zhu, C. S., Dai, W. T., Wang, K., Lin, C. S., Ni, H. Y., Corbin, J. C., Wu, Y. F., Zhang, R. J., Tie, X. X., Hoffmann, T., O'Dowd, C., and Dusek, U.: Brown carbon aerosol in urban Xi'an, Northwest China: the composition and light absorption properties, Environmental Science and Technology, 52(12), 6825–6833, 2018.

Jiang, Y. S., Gao, Y. H., He, C. L., Liu, B. L., Pan, Y. J., and Li, X.: Spatiotemporal distribution and variation of wind erosion over the Tibetan Plateau based on a coupled land-surface wind-erosion model, Aeolian Research, 50, 100699, 2021.

Kang, S. C., Zhang, Q. G., Qian, Y., Ji, Z. M., Li, C. L., Cong, Z. Y., Zhang, Y. L., Guo, J. M., Du, W. T., Huang, J., You, Q. L., Panday, A. K., Rupakheti, M., Chen, D. L., Gustafsson, O., Thiemens, M. H., and Qin, D. H.: Linking atmospheric pollution to cryospheric change in the Third Pole region: current progress and future prospects, National Science Review, 6(4), 796–809, 2019.

Kang, S. C., Zhang, Y. L., Qian, Y., and Wang, H. L.: A review of black carbon in snow and ice and its impact on the cryosphere, Earth-Science Reviews, 210, 103346, 2020.

Kawamura, K., Kasukabe, H., and Barrie, L. A.: Secondary formation of water-soluble organic acids and alpha-dicarbonyls and their contributions to total carbon and water-soluble organic carbon: Photochemical aging of organic aerosols in the Arctic spring, Journal of Geophysical Research: Atmospheres, 115, D21306, 2010.

Lau, W. K. M., Kim, M. K., Kim, K. M., and Lee, W. S.: Enhanced surface warming and accelerated snow melt in the Himalayas and Tibetan Plateau induced by absorbing aerosols, Environmental Research Letters, 5, 025204, 2010.

Li, C. L., Chen, P. F., Kang, S C., Yan, F. P., Hu, Z., Qu, B., and Sillanpää, M.: Concentrations and light absorption characteristics of carbonaceous aerosol in $PM_{2.5}$ and PM_{10} of Lhasa city, the Tibetan Plateau, Atmospheric Environment, 127, 340–346, 2016.

Liu, X. D., and Chen, B. D.: Climatic warming in the Tibetan Plateau during recent decades, International Journal of Climatology, 20(14), 1729–1742, 2000.

Liu, H., Pan, X. L., Liu, D. T., Liu, X., Chen, X., Tian, Y., Sun, Y. L., Fu, P. Q., and Wang, Z. F.: Mixing characteristics of refractory black carbon aerosols at an urban site in Beijing, Atmospheric Chemistry and Physics, 20, 5771–5785, 2020.

Liu, J. M., Scheuer, E., Dibb, J., Ziemba, L. D., Thornhill, K. L., Anderson, B. E., Wisthaler, A., Mikoviny, T., Devi, J. J., Bergin, M., and Weber, R. J.: Brown carbon in the continental troposphere, Geophysical Research Letters, 41, 2191–2195, 2014.

Liu, J., Scheuer, E., Dibb, J., Diskin, G. S., Ziemba, L. D., Thornhill, K. L., Anderson, B. E., Wisthaler, A., Mikoviny, T., Devi, J. J., Bergin, M., Perring, A. E., Markovic, M. Z., Schwarz, J. P., Campuzano-Jost, P., Day, D. A., Jimenez, J. L., and Weber, R. J.: Brown carbon aerosol in the North American continental troposphere: Sources, abundance, and radiative forcing, Atmospheric Chemistry and Physics, 15, 7841–7858, 2015.

Levinson, R., Akbari, H., and Berdahl, P.: Measuring solar reflectance—part I: defining a metric that

accurately predicts solar heat gain, Solar Energy, 84(9), 1717–1744, 2010.

Lu, A. G., Kang, S. C., Li, Z. X., and Theakstone, W. H.: Altitude effects of climatic variation on Tibetan Plateau and its vicinities, Journal of Earth Science, 21(2), 189–198, 2010.

Mountain Research Initiative EDW Working Group.: Elevation-dependent warming in mountain regions of the world, Nature Climate Change, 5(5), 424–430, 2015.

Olson, M. R., Garcia, M. V., Robinson, M. A., Rooy, P. V., Dietenberger, M. A., Bergin, M., and Schauer, J. J.: Investigation of black and brown carbon multiple-wavelength dependent light absorption from biomass and fossil fuel combustion source emissions, Journal of Geophysical Research: Atmospheres, 120(13), 6682–6697, 2015.

Palazzi, E., Filippi, L., and von Hardenberg, J.: Insights into elevation-dependent warming in the Tibetan Plateau-Himalayas from CMIP5 model simulations, Climate Dynamics, 48 (11), 3991–4008, 2017.

Peng, C., Yang, F. M., Tian, M., Shi, G. M., Li, L., Huang, R. J., Yao, X. J., Luo, B., Zhai, C. Z., and Chen, Y.: Brown carbon aerosol in two megacities in the Sichuan Basin of southwestern China: Light absorption properties and implications, Science of the Total Environment, 719, 137483, 2020a.

Peng, C., Tian, M., Wang, X. L., Yang, F. M., Shi, G. M., Huang, R. J., Yao, X. J., Wang, Q. Y., Zhai, C. Z. Zhang, S. M., Qian, R. Z., Cao, J. J., and Chen, Y.: Light absorption of brown carbon in $PM_{2.5}$ in the Three Gorges Reservoir region, southwestern China: Implications of biomass burning and secondary formation, Atmospheric Environment, 229, 117409, 2020b.

Pepin, N., Deng, H. J., Zhang, H. B., Zhang, F., Kang, S. C., and Yao, T. D.: An examination of temperature trends at high elevations across the Tibetan Plateau: The use of MODIS LST to understand patterns of elevation-dependent warming, Journal of Geophysical Research: Atmospheres, 124(11), 5738–5756, 2019.

Quick, D. J., and Chadwick, O. A.: Accumulation of salt-rich dust from Owens Lake playa in nearby alluvial soils, Aeolian Research, 3(1), 23–29, 2011.

Ramanathan, V., and Carmichael, G.: Global and regional climate changes due to black carbon, Nature Geoscience, 1(4), 221–227, 2008.

Rangwala, I., and Miller, J. R.: Climate change in mountains: a review of elevation-dependent warming and its possible causes, Climatic Change, 114(3-4), 527–547, 2012.

Srinivas, B., Rastogi, N., Sarin, M. M., Singh, A., and Singh, D.: Mass absorption efficiency of light

absorbing organic aerosols from source region of paddy-residue burning emissions in the Indo-Gangetic Plain, Atmospheric Environment, 125, 360–370, 2016.

Tao, J., Zhang, L. M., Zhang, R. J., Wu, Y. F., Zhang, Z. S., Zhang, X. L., Tang, Y. X., Cao, J. J., and Zhang, Y. H.: Uncertainty assessment of source attribution of $PM_{2.5}$ and its water-soluble organic carbon content using different biomass burning tracers in positive matrix factorization analysis-a case study in Beijing, China, Science of the Total Environment, 543, 326–335, 2016.

Tian, P. F., Zhang, L., Ma, J. M., Tang, K., Xu, L. L., Wang, Y., Cao, X. J., Liang, J. N., Ji, Y. M., Jiang, J. H., Yung, Y. L., and Zhang, R. Y.: Radiative absorption enhancement of dust mixed with anthropogenic pollution over East Asia, Atmospheric Chemistry and Physics, 18(11), 7815–7825, 2018.

Turpin, B. J., and Lim, H. J.: Species contributions to $PM_{2.5}$ mass concentrations: revisiting common assumptions for estimating organic mass, Aerosol Science and Technology, 35(1), 602−610, 2001.

Viidanoja, J., Sillanpaa, M., Laakia, J., Kerminen, V. M., Hillamo, R., Aarnio, P., and Koskentalo, T.: Organic and black carbon in $PM_{2.5}$ and PM_{10}: 1 year of data from an urban site in Helsinki, Finland, Atmospheric Environment, 36(19), 3183−3193, 2002.

Wang, H. B., Tian, M., Chen, Y., Shi, G. M., Liu, Y., Yang, F. M., Zhang, L. M., Deng, L. Q., Yu, J., Peng, C., and Cao, X. Y.: Seasonal characteristics, formation mechanisms and source origins of $PM_{2.5}$ in two megacities in Sichuan Basin, China, Atmospheric Chemistry and Physics, 18(2), 865−881, 2018.

Wang, Y. J., Hu, M., Hu, W., Zheng, J., Niu, H. Y., Fang, X., Xu, N., Wu, Z. J., Guo, S., Wu, Y. S., Chen, W. T., Lu, S. H., Shao, M., Xie, S. D., Luo, B., and Zhang, Y. H.: Secondary formation of aerosols under typical high-humidity conditions in wintertime Sichuan Basin, China: A contrast to the North China Plain, Journal of Geophysical Research: Atmospheres, 126(10), e2021JD034560, 2021.

Wilson, J. G., Kingham, S., Pearce, J., and Sturman, A. P.: A review of intraurban variations in particulate air pollution: implications for epidemiological research, Atmospheric Environment, 39(34), 6444−6462, 2005.

Wu, G. M., Wan, X., Gao, S. P., Fu, P. Q., Yin, Y. G., Li, G., Zhang, G. S., Kang, S. C., Ram, K., and Cong, Z. Y.: Humic-like substances (HULIS) in aerosols of central Tibetan Plateau (Nam Co, 4730 m asl): abundance, light absorption properties, and sources, Environmental Science and Technology, 52(13), 7203−7211, 2018.

Xu, B. Q., Cao, J. J., Hansen, J., Yao, T. D., Joswia, D. R., Wang, N. L., Wu, G. J., Wang, M., Zhao, H. B., Yang, W., Liu, X. Q., and He, J. Q.: Black soot and the survival of Tibetan glaciers, Proceedings of

the National Academy of the Sciences of the United States of America, 106(52), 22114–22118, 2009.

Yin, D. Y., Zhao, S. P., Qu, J. J., Yu, Y., Kang, S. C., Ren, X. L., Zhang, J., Zou, Y., Dong, L. X., Li, J. L., He, J. J., Li, P., and Qin, D. H.: The vertical profiles of carbonaceous aerosols and key influencing factors during wintertime over western Sichuan Basin, China, Atmospheric Environment, 223, 117269, 2020.

You, Q. L., Chen, D. L., Wu, F. Y., Pepin, N., Cai, Z. Y., Ahrens, B., Jiang, Z. H., Wu, Z. W., Kang, S. C., and AghaKouchak A.: Elevation dependent warming over the Tibetan Plateau: Patterns, mechanisms and perspectives, Earth-Science Reviews, 210, 103349, 2020.

Zeng, L. H., Zhang, A. X., Wang, Y. H., Wagner, N. L., Katich, J. M., Schwarz, J. P., Schill, G. P., Brock, C., Froyd, K. D., Murphy, D. M., Williamson, C. J., Kupc, A., Scheuer, E., Dibb, J., and Weber, R. J.: Global measurements of brown carbon and estimated direct radiative effects, Geophysical Research Letters, 47(13), e2020GL088747, 2020.

Zhang, J., Wang, Y. Y., Teng, X. M., Liu, L., Xu, Y. S., Ren, L. H., Shi, Z. B., Zhang, Y., Jiang, J. K., Liu, D. T., Hu, M., Shao, L. Y., Chen, J. M., Martin, S. T., Zhang, X. Y., and Li, W. J.: Liquid-liquid phase separation reduces radiative absorption by aged black carbon aerosols, Communications Earth & Environment, 3, 128, 2022.

Zhang, L., Tang, C. G., Huang, J. P., Du, T., Guan, X., Tian, P. F., Shi, J. S., Cao, X. J., Huang, Z. W., Guo, Q., Zhang, H. T., Wang, M., Zeng, H. Y., Wang, F. Y., and Dolkar, P.: Unexpected high absorption of atmospheric aerosols over a western Tibetan Plateau site in summer, Journal of Geophysical Research: Atmospheres, 126(7), e2020JD033286, 2021.

Zhang, X. Y., Zhuang, G. S., Yuan, H., Rahn, K. A., Wang, Z. F., and An, Z. S.: Aerosol particles from dried salt-lakes and saline soils carried on dust storms over Beijing, Terrestrial Atmospheric and Oceanic Sciences, 20(4), 619–628, 2009.

Zhang, Y. Z., Forrister, H., Liu, J. M., Dibb, J., Anderson, B., Schwarz, J. P., Perring, A. E., Jimenez, J. L., Campuzano-Jost, P., Wang, Y. H., Nenes, A., and Weber, R. J.: Top-of-atmosphere radiative forcing affected by brown carbon in the upper troposphere, Nature Geoscience, 10(7), 486–489, 2017.

Zhao, C. F., Yang, Y. K., Fan, H., Huang, J. P., Fu, Y. F., Zhang, X. Y., Kang, S. C., Cong, Z. Y., Letu, H., and Menenti, M.: Aerosol characteristics and impacts on weather and climate over the Tibetan Plateau, National Science Review, 7(3), 492–495, 2020.

Zhao, S. P., Yu, Y., Yin, D. Y., Qin, D. H., He, J. J., and Dong, L. X.: Spatial patterns and temporal

variations of six criteria air pollutants during 2015 to 2017 in the city clusters of Sichuan Basin, China, Science of the Total Environment, 624, 540–557, 2018.

Zhao, S. P., Yin, D. Y., Yu, Y., Kang, S. C., Ren, X. L., Zhang, J., Zou, Y., and Qin, D. H.: PM_1 chemical composition and light absorption properties in urban and rural areas within Sichuan Basin, southwest China, Environmental Pollution, 280, 116970, 2021.

Zhao, S. P., Qi, S. F., Yu, Y., Kang, S. C., Dong, L. X., Chen, J. B., and Yin, D. Y.: Measurement report: The first *in-situ* PM1 chemical measurements at the steep slope from highly polluted Sichuan Basin to pristine Tibetan Plateau: light absorption of carbonaceous aerosols, and source and origin impacts [data set], https://doi.org/10.5281/zenodo.6474199, 2022.

Zhao, S. Y., Feng, T., Tie, X. X., and Wang, Z. B.: The warming Tibetan Plateau improves winter air quality in the Sichuan Basin, China, Atmospheric Chemistry and Physics, 20(23), 14873–14887, 2020.

Zhao, Z. Z., Cao, J. J, Chow, J. C., Watson, J. G., Chen, A. L.-W., Wang, X. L., Wang, Q. Y., Tian, J., Shen, Z. X., Zhu, C. S., Liu, S. X., Tao, J., Ye, Z. L., Zhang, T., Zhou, J. M., and Tian, R. X.: Multi-wavelength light absorption of black and brown carbon at a high-altitude site on the Southeastern margin of the Tibetan Plateau, China, Atmospheric Environment, 212, 54–64, 2019.

Zhu, C. S., Cao, J. J., Huang, R. J., Shen, Z. X., Wang, Q. Y., and Zhang, N. N.: Light absorption properties of brown carbon over the southeastern Tibetan Plateau, Science of the Total Environment, 625, 246–251, 2018.

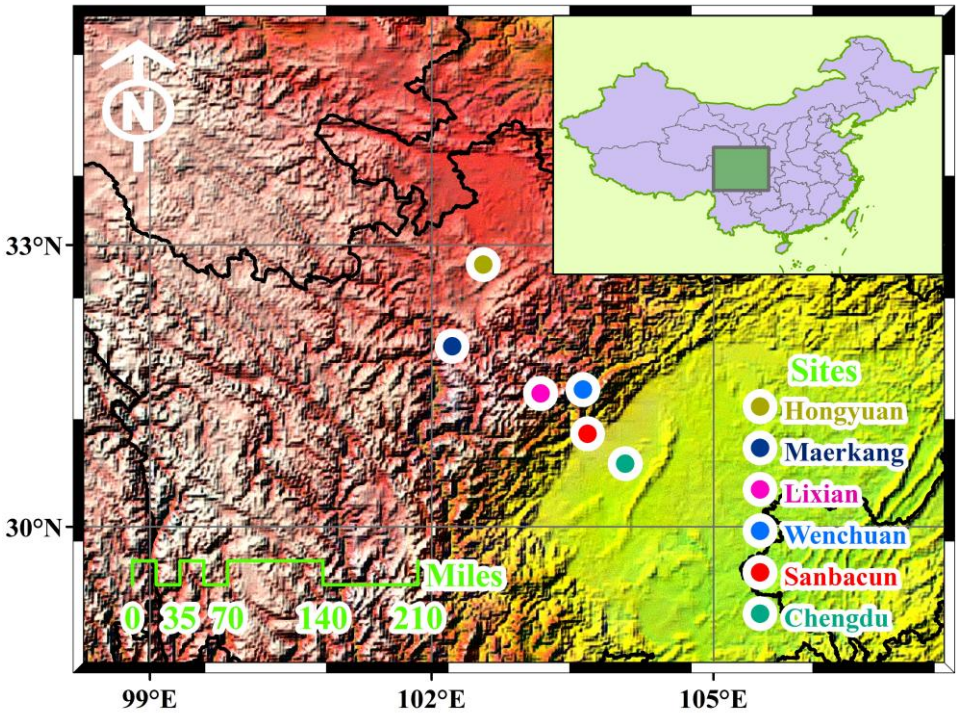

Figure 1: Geographic location of the six *in -situ* measurement sites (Chengdu, Sanbacun, Wenchuan, Lixian, Maerkang, and Hongyuan) along the ~~eastern slope of Tibetan Plateau~~ESTP. The map is a pure reproduction of Google Maps with added a marks for our study locations. Copyright © Google Maps.

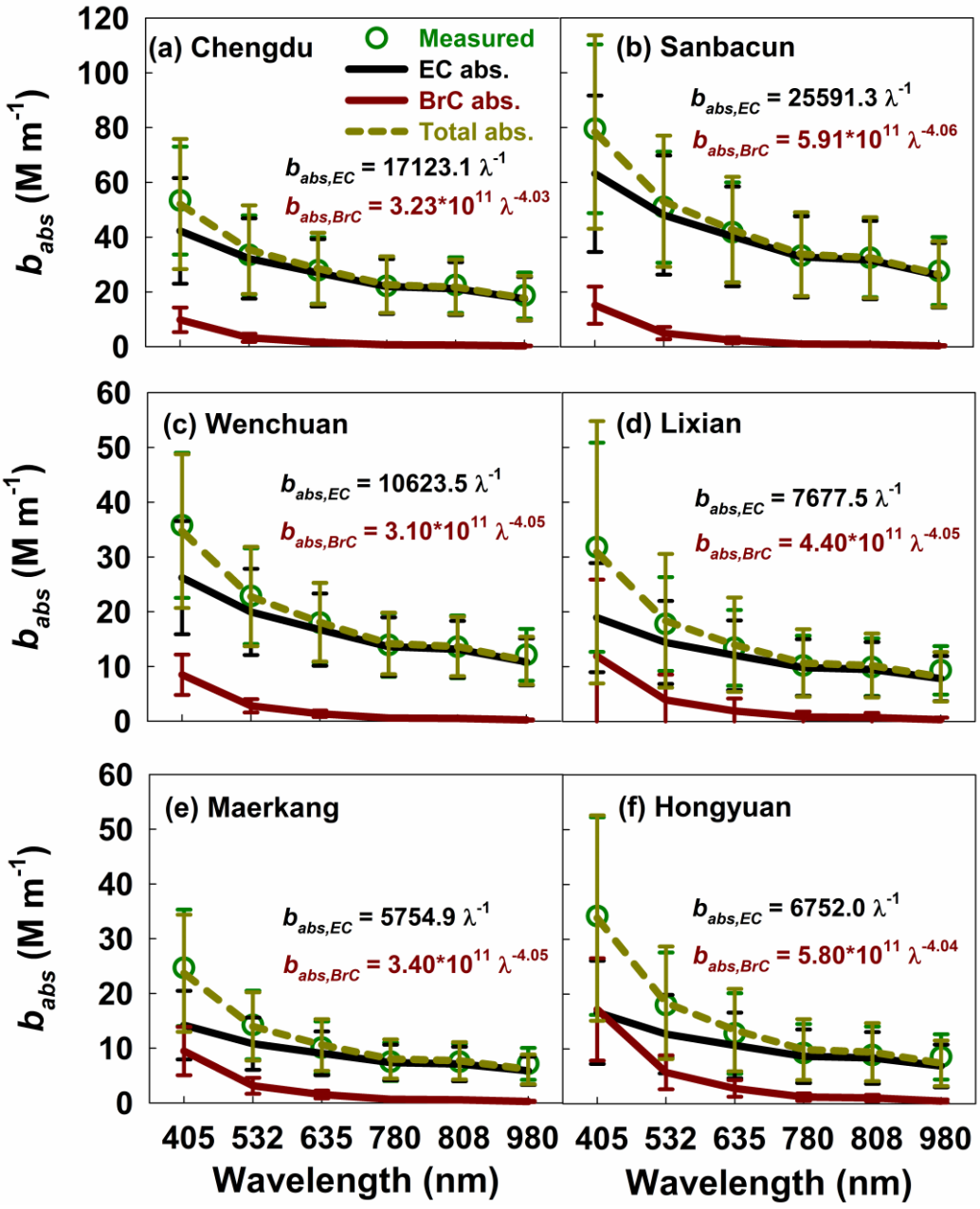

Figure 2: Spectral light absorption coefficients (b_{abs}) by EC and BrC in spring and winter at the six sites along the ESTP. The subplots depict the decomposition of total light absorption by EC and BrC with the model given in Eq. 4. Error bars represent uncertainties derived from replicate analyses and lower quantifiable limits.

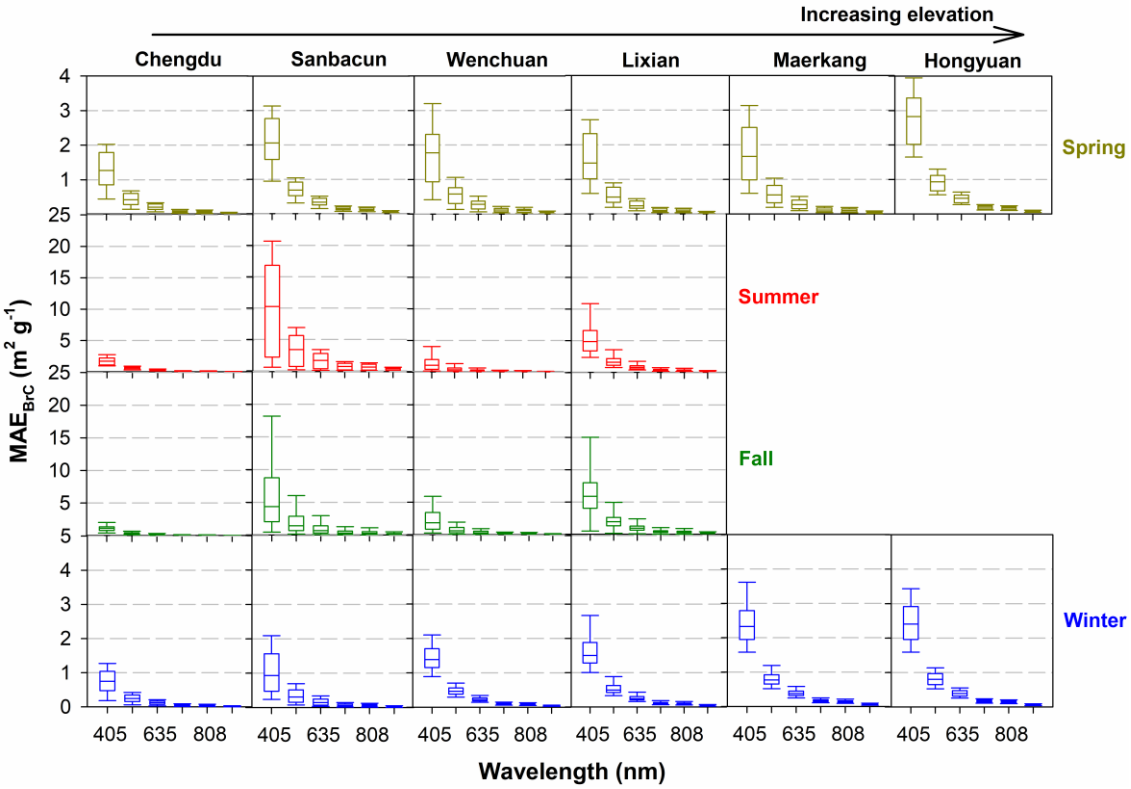

Figure 3: Box plots of spectral ~~BrC~~ mass absorption efficiency of BrC (MAE_{BrC}) in each season from Chengdu inside the SCB to Hongyuan over the TP ~~extending~~ ranging in elevation from 500 m to 3500 m. The lines inside the boxes denote the median values, and the two whiskers and the top and bottom of the boxes denote the 5th and 95th and the 75th and 25th percentiles.

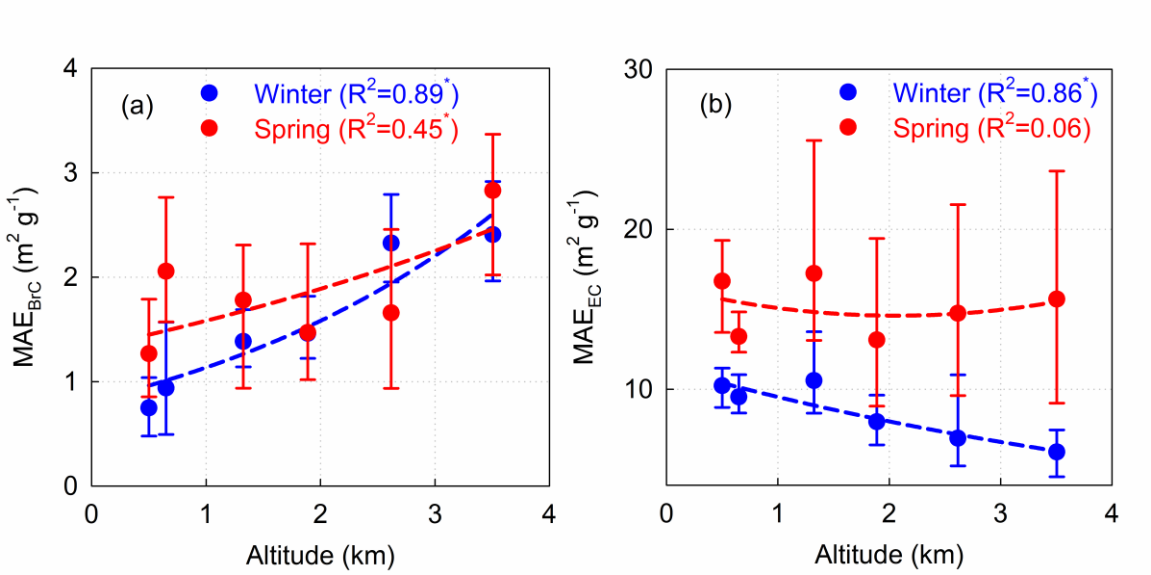

Figure 4: Variations of (a) MAE_{BrC} and (b) MAE_{EC} at 405 nm as altitude in spring and winter during the field campaign. The solid dots denote the median values, and the two whiskers of the dots denote the 25th and 75th percentiles. The relationships between averaged MAE and altitude of the measurement sites were fitted by exponential function, and the coefficients of determination (R^2) also were given in each subplot. The relationships (R^2 with the superscript of an asterisk) passed the significance level of 0.01.

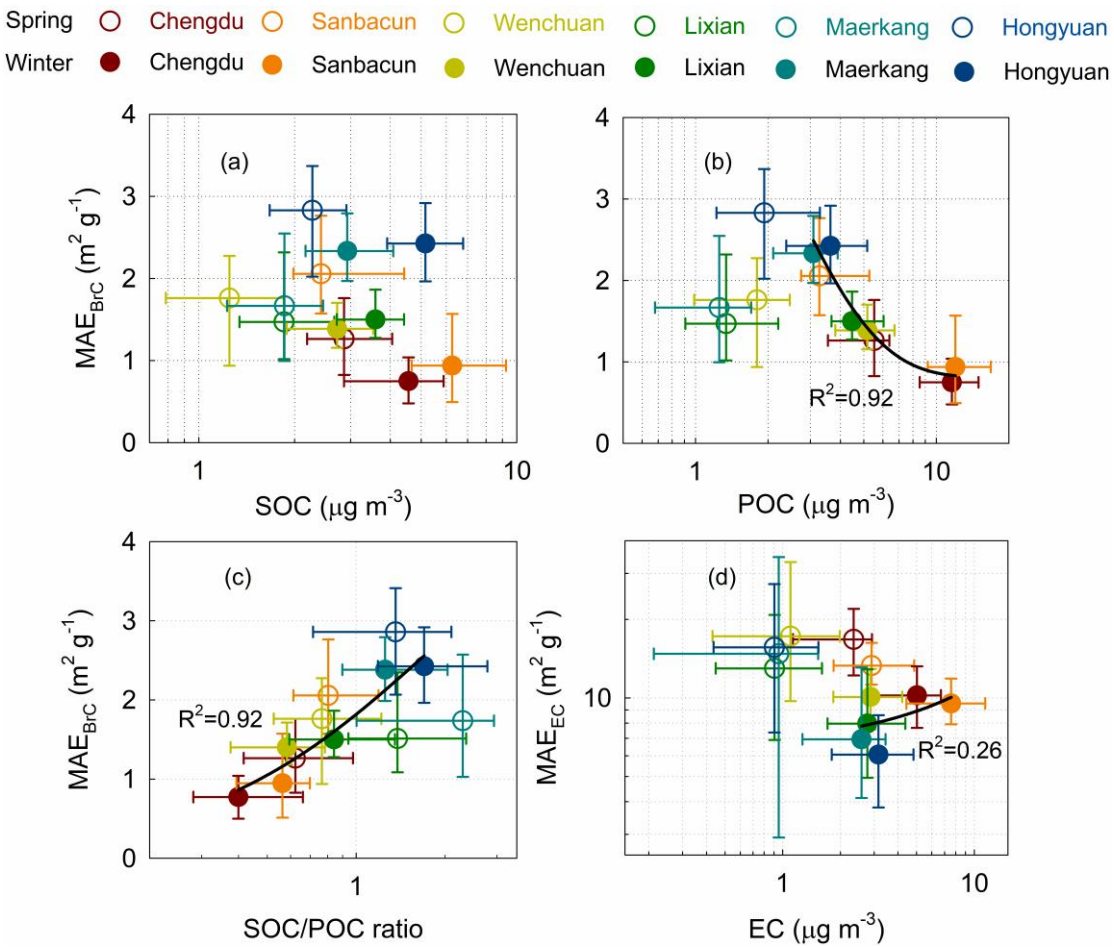

Figure 5: Variations of ~~spring and winter mean~~ averaged MAE_{BrC} in spring and winter as (a) SOC, (b) POC, (c) SOC/POC ratio and (d) MAE_{EC} as EC concentrations at the six sites. The hollow and solid dots denote the median values in spring and winter, and the four whiskers of the dots denote the 25th and 75th percentiles of the corresponding two variables. The horizontal axis in each subplot is showed on a logarithmic scale to more clearly see the details.

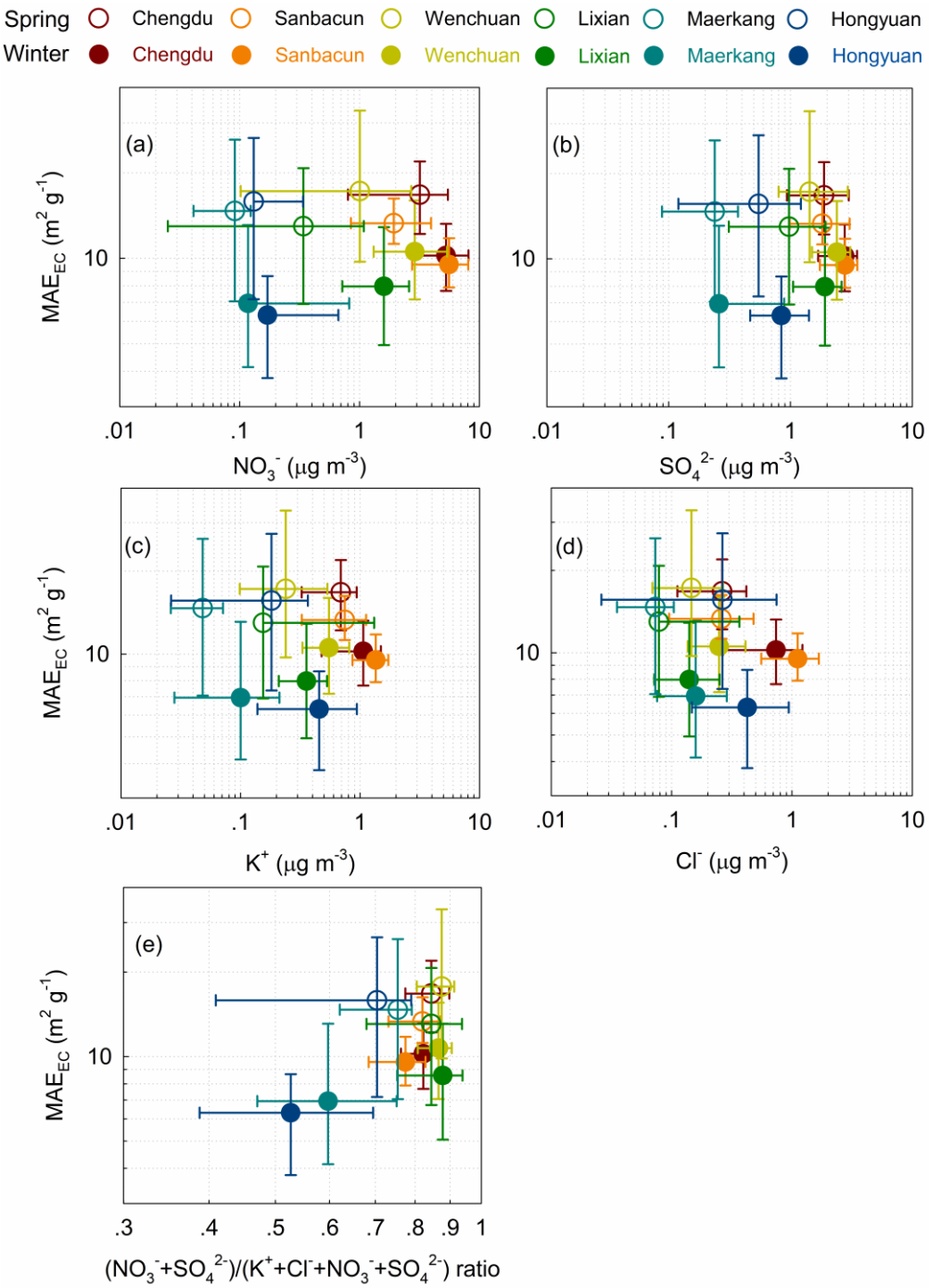

Figure 6: Variations of ~~spring and winter~~ MAE_{EC} in spring and winter as (a) NO_3^-, (b) SO_4^{2-}, (c) K^+, and (d) Cl^- concentrations, and (e) $(NO_3^-+ SO_4^{2-})$ / $(K^+ + Cl^- + NO_3^- + SO_4^{2-})$ ratio at the six sites. The hollow and solid dots denote the median values in spring and winter, and the four whiskers of the dots denote the 25th and 75th percentiles of the corresponding two variables. The axes in each subplot are showed on a logarithmic scale to more clearly see the details.

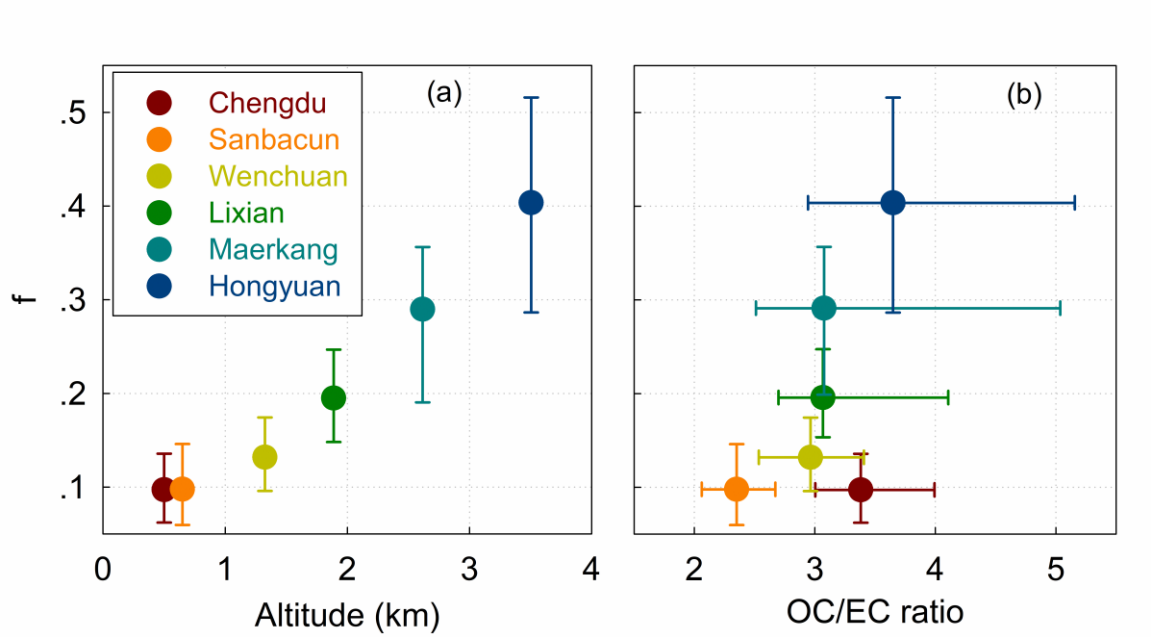

Figure 7: Variation of radiative forcing of BrC relative to EC (f, see Eq. 8) as (a) altitude and (b) OC/EC ratio for each site. The solid dots denote the median values, and the two whiskers of the dots denote the 25th and 75th percentiles of the variables.

5

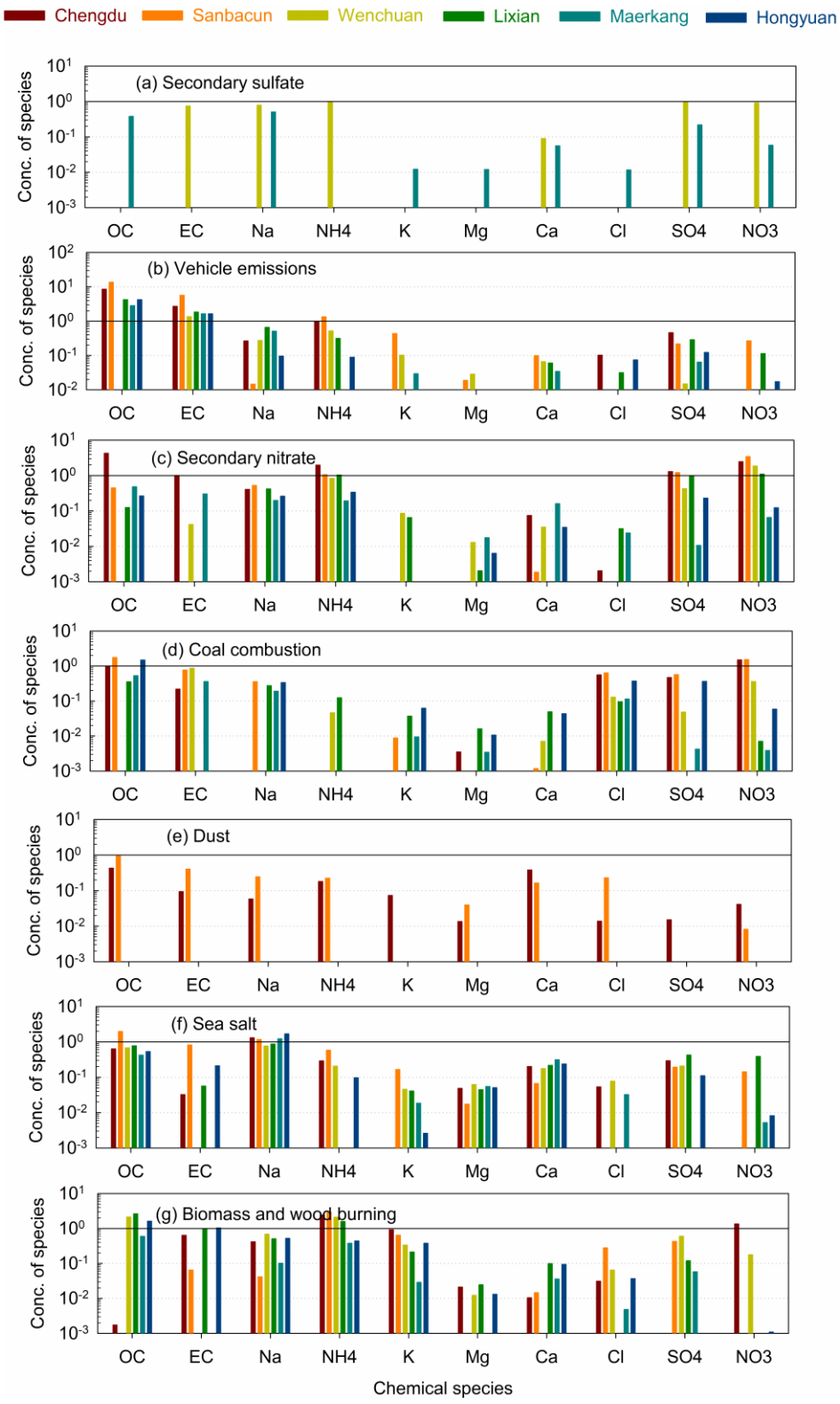

Figure 8: Mass concentrations of species for each source at each site apportioned by PMF model in winter during the campaign. The vertical axes are showed on logarithmic scale to better distinguish the concentrations of chemical species among the measurement sites.

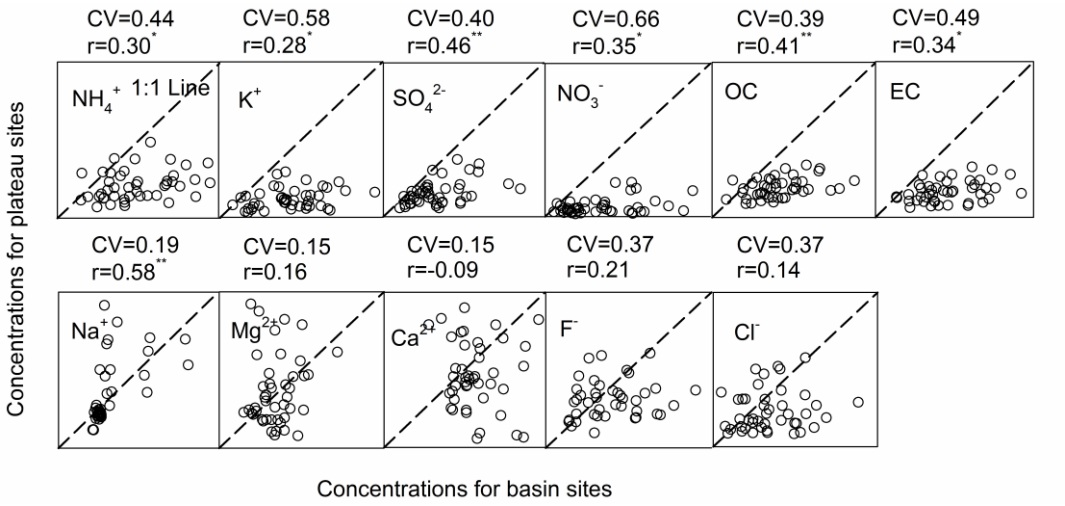

Figure 9: Relationships of ~~spring~~ PM_1 chemical components concentrations in spring between basin (horizontal axes, including Chengdu and Sanbacun) and plateau sites (vertical axes, including Wenchuan, Lixian, Maerkang and Hongyuan). The correlation coefficients (r) with an asterisk and two asterisk superscripts passed the significance level of 0.05 and 0.01, respectively.

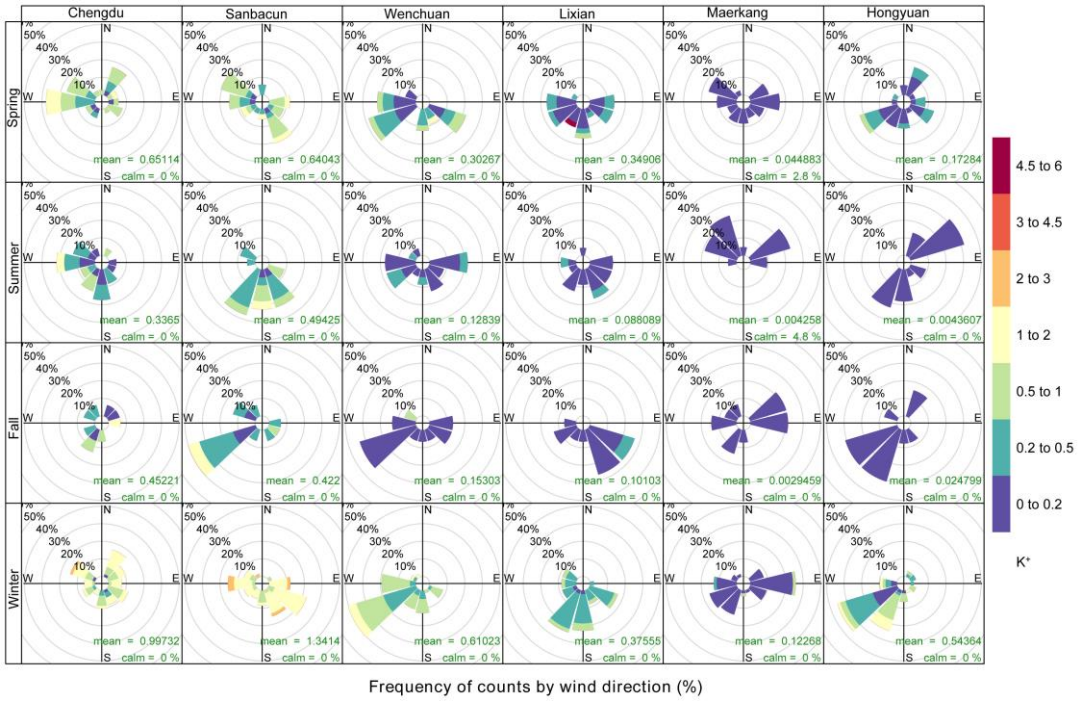

Figure 10: K^+ pollution rose in the four seasons at the six sites along the ESTP. Mean K^+ concentrations and calm frequencies also were given in each subplot.

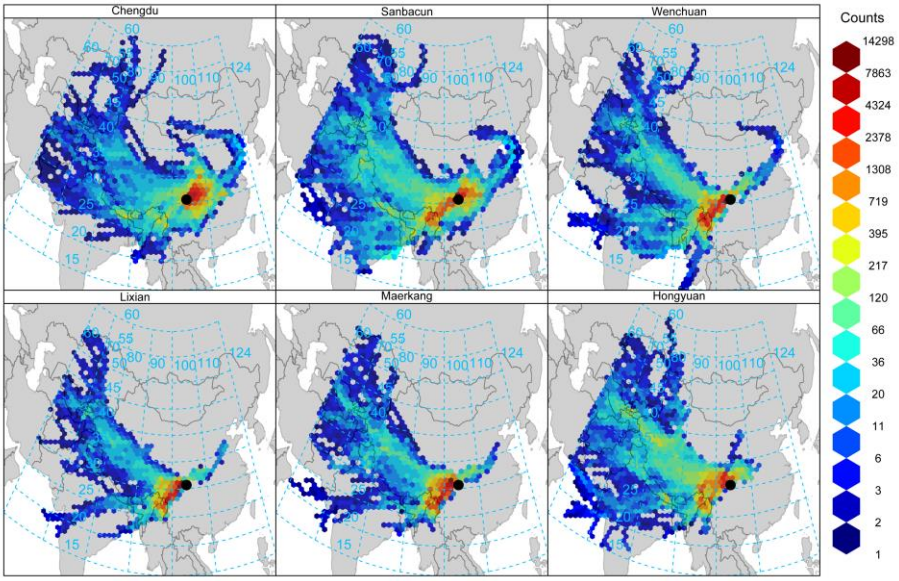

Figure 11: Gridded back trajectory frequencies with hexagonal binning in winter at the six sites from west Sichuan Basin to Tibetan Plateau. The map is a pure reproduction of Google Maps with added the trajectory frequencies. Copyright © Google Maps.

Table 1 Summary of the measurement sites (name, location and altitude).

Name	Latitude (degree)	Longitude (degree)	Altitude (km)
Chengdu	30.67	104.06	0.50
Sanbacun	30.99	103.66	0.65
Wenchuan	31.46	103.61	1.33
Lixian	31.42	103.16	1.89
Maerkang	31.92	102.22	2.62
Hongyuan	32.79	102.55	3.50

Table2 Seasonally averaged values (mean ± std.) of OC and EC concentrations, light absorption coefficient (b_{abs}), mass absorption efficiency (MAE) and meteorological variables (wind speed (WS), temperature (Tem.), relative humidity (RH)) at the six sites during the measurement campaign. There is no b_{abs} or MAE reported for MEK and HY in summer and fall as the used DRI instrument does not work at the 2 wavelengths of 405 nm and 445 nm when the samples are measured, and thus separation of EC and BrC cannot be conducted by Eq. (5). Chengdu, Sanbacun, Wenchuan, Lixian, Maerkang and Hongyuan are abbreviated as CD, SBC, WC, LX, MEK and HY, respectively.

Season	Sites	OC	EC	b_{abs} (M m^{-1})		MAE (m^2 g^{-1})		WS	Tem.	RH
		(μg m^{-3})	(μg m^{-3})	BrC, 405	EC, 405	BrC, 405	EC, 405	(m s^{-1})	(℃)	(%)
Spring	CD	7.9±3.7	2.2±1.2	8.5±2.8	32.4±12.7	1.3±0.6	17.1±4.8	1.6±0.7	17.5±4.3	80.3±19.9
	SBC	6.7±3.0	3.3±1.5	13.7±5.6	44.2±16.9	2.1±0.9	13.7±2.5	1.4±0.6	16.9±4.1	77.6±15.9
	WC	3.2±1.6	1.2±0.8	4.8±2.3	20.2±9.0	1.6±0.9	21.5±11.6	2.4±1.0	15.1±4.4	65.1±17.4
	LX	3.5±1.4	1.0±0.6	5.4±2.5	11.8±5.5	1.7±0.8	13.8±6.9	1.6±0.5	13.3±5.3	61.5±20.4
	MEK	3.0±1.7	0.8±0.6	4.8±2.7	10.2±3.6	1.9±1.2	16.6±9.4	1.1±0.6	10.6±5.5	62.0±26.5
	HY	4.1±1.6	0.9±0.6	11.5±4.9	12.9±6.2	2.8±0.9	17.3±9.8	2.4±1.0	2.4±3.6	70.0±16.6
Summer	CD	5.4±1.2	1.9±0.5	9.0±2.7	29.2±6.9	1.8±0.6	16.4±4.5	1.3±0.4	25.2±2.9	84.6±18.8
	SBC	2.9±1.2	1.5±0.7	21.8±15.0	32.6±7.9	10.1±7.1	29.8±6.5	1.1±0.4	24.1±3.0	82.7±13.9
	WC	2.2±0.8	1.0±0.5	2.2±1.5	18.9±5.5	1.4±1.3	23.5±9.5	1.7±0.7	23.1±3.2	64.5±16.5
	LX	2.7±0.9	0.8±0.5	13.3±5.0	9.5±2.7	5.4±2.5	16.4±11.3	1.4±0.5	20.9±4.0	65.2±18.0
	MEK	2.7±1.5	0.7±0.6	—	—	—	—	1.0±0.4	16.6±4.3	73.3±22.6
	HY	3.0±1.2	0.8±0.6	—	—	—	—	1.8±0.6	10.1±3.3	77.8±11.6
Fall	CD	4.7±1.3	2.3±1.0	5.3±2.5	40.6±16.6	1.1±0.5	18.3±4.0	1.1±0.4	15.6±4.9	88.4±10.8
	SBC	5.3±3.4	3.0±1.8	22.0±13.7	50.8±11.2	6.0±5.6	24.3±9.3	0.9±0.2	14.9±4.4	89.9±11.6
	WC	1.6±0.8	0.8±0.5	3.0±2.0	18.2±7.3	2.3±1.8	27.3±13.9	1.7±0.6	14.1±5.4	72.7±10.0
	LX	2.4±1.0	0.9±0.5	12.7±6.6	10.5±3.4	6.5±3.8	14.7±10.1	1.3±0.3	11.9±5.6	76.8±11.3
	MEK	2.3±1.2	0.9±0.6	—	—	—	—	0.9±0.4	8.8±5.5	78.4±17.0
	HY	3.4±2.2	1.3±1.1	—	—	—	—	1.9±0.7	0.7±5.6	73.9±11.0
Winter	CD	15.0±5.9	4.7±2.0	10.5±4.6	47.6±20.1	0.8±0.5	10.4±2.8	1.2±0.4	6.6±2.7	78.9±16.9
	SBC	18.9±7.6	7.9±3.4	17.1±10.2	74.7±27.9	1.2±1.0	9.9±2.0	1.0±0.3	5.8±2.7	79.2±15.0
	WC	8.2±3.1	2.8±1.3	11.2±3.2	29.7±9.5	1.5±0.5	11.6±4.4	1.9±0.6	3.6±2.4	60.2±9.0
	LX	8.4±2.7	3.0±1.3	17.1±15.4	24.3±9.1	2.2±2.6	8.9±3.9	1.4±0.4	-0.1±2.1	62.4±10.3
	MEK	5.3±2.3	2.2±1.1	13.2±4.0	16.6±6.3	2.5±0.9	8.6±4.4	1.1±0.3	-0.2±3.7	36.1±11.0
	HY	8.4±3.8	3.0±1.6	21.5±11.3	18.9±10.2	2.5±0.7	6.7±4.9	2.1±1.5	-6.5±6.8	42.8±21.8